doi:10.1016/j.jmb.2010.08.045 J. Mol. Biol. (2010) 403, 351–370

Contents lists available at www.sciencedirect.com

Journal of Molecular Biology

journal homepage: http://ees.elsevier.com.jmb

A Structural Hinge in Eukaryotic MutY Homologues Mediates Catalytic Activity and Rad9–Rad1–Hus1 Checkpoint Complex Interactions

Paz J. Luncsford[1]†, Dau-Yin Chang[1]†, Guoli Shi[1], Jade Bernstein[1], Amrita Madabushi[1], Dimeka N. Patterson[1], A-Lien Lu[1,2]* and Eric A. Toth[1,2]*

[1]*Department of Biochemistry and Molecular Biology, University of Maryland School of Medicine, 108 North Greene Street, Baltimore, MD 21201, USA*
[2]*Marlene and Stewart Greenebaum Cancer Center, University of Maryland School of Medicine, 108 North Greene Street, Baltimore, MD 21201, USA*

Received 15 June 2010; received in revised form 25 August 2010; accepted 25 August 2010
Available online 15 September 2010

Edited by M. F. Summers

Keywords:
DNA glycosylase;
DNA repair;
cell cycle checkpoint;
Rad9–Rad1–Hus1;
crystal structure

The DNA glycosylase MutY homologue (MYH or MUTYH) removes adenines misincorporated opposite 8-oxoguanine as part of the base excision repair pathway. Importantly, defects in human MYH (hMYH) activity cause the inherited colorectal cancer syndrome MYH-associated polyposis. A key feature of MYH activity is its coordination with cell cycle checkpoint via interaction with the Rad9–Rad1–Hus1 (9-1-1) complex. The 9-1-1 complex facilitates cell cycle checkpoint activity and coordinates this activity with ongoing DNA repair. The interdomain connector (IDC, residues 295–350) between the catalytic domain and the 8-oxoguanine recognition domain of hMYH is a critical element that maintains interactions with the 9-1-1 complex. We report the first crystal structure of a eukaryotic MutY protein, a fragment of hMYH (residues 65–350) that consists of the catalytic domain and the IDC. Our structure reveals that the IDC adopts a stabilized conformation projecting away from the catalytic domain to form a docking scaffold for 9-1-1. We further examined the role of the IDC using *Schizosaccharomyces pombe* MYH as model system. *In vitro* studies of *S. pombe* MYH identified residues I261 and E262 of the IDC (equivalent to V315 and E316 of the hMYH IDC) as critical for maintaining the MYH/9-1-1 interaction. We determined that the eukaryotic IDC is also required for DNA damage selection and robust enzymatic activity. Our

**Corresponding authors.* Department of Biochemistry and Molecular Biology, University of Maryland School of Medicine, 108 North Greene Street, Baltimore, MD 21201, USA. E-mail addresses: aluchang@umaryland.edu; etoth001@umaryland.edu.

† P.J.L. and D.-Y.C. contributed equally to this work.

Present address: G. Shi, Office of Research, University of Maryland School of Nursing, 655 West Lombard Street, Baltimore, MD 21201, USA.

Abbreviations used: MYH, MutY homologue; hMYH, human MYH; 9-1-1, Rad9–Rad1–Hus1; IDC, interdomain connector; 8-oxoG, 7,8-dihydro-8-oxoguanine; SpMyh1, *Schizosaccharomyces pombe* MYH; BER, base excision repair; AP, apurinic/apyrimidinic; APE1, AP endonuclease 1; MAP, MYH-associated polyposis; PCNA, proliferating cell nuclear antigen; H_2O_2, hydrogen peroxide; EcMutY, *Escherichia coli* MutY; BstMutY, *Bacillus stearothermophilus* MutY; HhH, helix–hairpin–helix; GST, glutathione *S*-transferase; WT, wild type; GFP, green fluorescence protein; MBP, maltose-binding protein; EDTA, ethylenediaminetetraacetic acid; DEAE, diethylaminoethyl; EMM, Edinburgh minimal medium; YNB, yeast nitrogen base; FOA, 5-fluoro-orotic acid.

studies also provide the first evidence that disruption of the MYH/9-1-1 interaction diminishes the repair of oxidative DNA damage *in vivo*. Thus, preserving the MYH/9-1-1 interaction contributes significantly to minimizing the mutagenic potential of oxidative DNA damage.

Introduction

The genome is vulnerable to DNA-damaging agents of both endogenous and environmental origin. Guanine is very susceptible to oxidation and can be converted into 7,8-dihydro-8-oxoguanine (8-oxoG), which is one of the most stable and deleterious products of oxidative DNA damage.[1] There are approximately 10^3 and 10^5 8-oxoG lesions per cell per day in normal and cancerous tissues, respectively.[2] Importantly, if 8-oxoG is not repaired, adenine is misincorporated opposite 8-oxoG during DNA replication,[3] ultimately leading to G:C → T:A mutations within the genome.[4–6]

Eukaryotic MutY homologues (MYH or MUTYH) such as human MYH (hMYH) and *Schizosaccharomyces pombe* MYH (SpMyh1) are vital DNA glycosylases that carry out the first step in the base excision repair (BER) pathway to excise adenines or 2-hydroxyadenines mispaired with 8-oxoGs or guanines. MYH cleaves the *N*-glycosidic bond between the target base and its deoxyribose sugar, leaving an apurinic/apyrimidinic (AP) site.[7] The phosphodiester bond 5′ to the AP site is then cleaved by AP endonuclease 1 (APE1), and downstream BER enzymes complete the repair process. The functional importance of MYH is observed both experimentally and clinically: (1) deletion of Sp*myh1*$^{+}$[8] or mouse *MYH*[9] genes results in a substantial increase in mutation rate *in vivo*, and (2) biallelic *hMYH* mutations permit downstream mutations in tumor suppressors (i.e., APC) and protooncogenes (i.e., K-ras), causing colorectal adenomas and carcinomas [as in the syndrome MYH-associated polyposis (MAP)].[10–13] To date, 85 MAP-associated mutations spread throughout the entire length of the gene have been identified.[14] However, only 11 MAP-associated hMYH variants have been characterized via functional studies;[14–18] among these, only 3 variants (V232F and Q324R/H) have mutations within putative protein interaction domains. Additional studies must be performed to investigate the potential involvement of impaired protein interactions with hMYH variants in the development of colorectal cancer in some MAP patients.

In eukaryotes, detection and correction of DNA damage are coordinated, through protein–protein interactions, with signaling pathways that regulate DNA replication, cell cycle progression, and apoptosis.[19,20] We have shown that MYH directly associates with proliferating cell nuclear antigen (PCNA) in both *S. pombe* cells and human cells.[21,22] We also provided direct evidence that the association between SpMyh1 and PCNA is biologically important for SpMyh1 function in mutation avoidance.[21] The association between MYH and PCNA is believed to direct repair towards daughter DNA strands by coupling the BER pathway with DNA replication.[21–25] The connection between DNA repair and cell cycle checkpoints provides an additional mechanism to preserve genomic integrity.[20] In response to DNA damage, checkpoint proteins initiate cell cycle arrest to allow more time for enhanced DNA repair. In cases of extreme DNA damage, apoptosis can be triggered.

Checkpoint controls are highly conserved from yeast to humans. In fission yeast *S. pombe*, six checkpoint sensor proteins (Rad9, Rad1, Hus1, Rad17, Rad3, and Rad26) are proposed to initiate proper DNA damage response under DNA replication block or stress.[26,27] Rad9, Rad1, and Hus1 form a heterotrimeric complex [the Rad9–Rad1–Hus1 (9-1-1) complex]. The structure of the 9-1-1 complex was recently determined[28–30] and exhibited a striking structural similarity with the PCNA sliding clamp.[31–33] Besides serving as a damage sensor,[34–36] the 9-1-1 complex has been shown to interact with and stimulate many enzymes in the BER repair pathway.[37] During normal DNA replication, MYH coordinates with PCNA; however, in the event of DNA damage, MYH is proposed to recruit the 9-1-1 complex, which then enhances MYH glycosylase activity.[38,39] Importantly, mammalian cell cycle checkpoint proteins are recognized as key tumor suppressors,[40] and their direct role in DNA repair, such as with the MYH/9-1-1 interaction, can prevent accumulation of mutations.

Although bacterial MutY structures have been published,[41,42] MYH contains extra sequence information that encodes for structural domains that mediate its interactions with enzymes involved in DNA replication, mismatch repair, and cell cycle checkpoints.[37] As the checkpoint response is unique to eukaryotes, the region of MYH that is critical for interaction with the 9-1-1 complex is absent in the prokaryotic enzyme. We have shown that the major 9-1-1 binding site is located within residues 295–350 of hMYH and residues 245–293 of SpMyh1.[39] In this study, we use structural and biochemical approaches to further examine the interaction between MYH and the 9-1-1 complex, and its significance to DNA repair. Here we report the first eukaryotic structure of MYH containing the

hMYH catalytic domain and the 9-1-1 binding region [within the interdomain connector (IDC)]. The structure of hMYH (residues 65–350) has been solved to 2.3 Å resolution and shows that the IDC differs in size and orientation from its bacterial counterparts. We further examined the significance of the interaction between the SpMyh1 IDC and the 9-1-1 complex. We previously determined that mutation of V315 of hMYH and mutation of I261 of SpMyh1 attenuate the interaction with 9-1-1[39] to a modest extent. In an attempt to elicit a biological effect *in vivo*, we mutated the adjacent highly conserved glutamate to glutamine (E262Q). In this report, we demonstrate that residues I261 and E262 of SpMyh1 are key mediators of its interaction with the 9-1-1 complex and that disruption of the interaction itself hinders DNA repair *in vivo*. In particular, the SpMyh1(I261A/E262Q) mutant cannot complement the mutator phenotype of *myh1*Δ cells, and interruption of the interaction between SpMyh1 and 9-1-1 increases cell sensitivity to hydrogen peroxide (H_2O_2). To further examine the role of the IDC in MYH function, we created an SpMyh1-Chimera construct that included the N-terminal and C-terminal domains of SpMyh1 but replaced the IDC with the *Escherichia coli* MutY (EcMutY) linker region. We determined that although the IDC of SpMyh1 is not needed for DNA binding, it is required for DNA substrate selection and robust enzymatic activity of the eukaryotic protein. Our results demonstrate that the interaction between MYH and the 9-1-1 complex is an important step in DNA repair. Furthermore, these results strengthen the possibility that impaired hMYH–protein interactions contribute to the development of colorectal cancer in some MAP patients.

Results

hMYH(65–350) contains the six-helix barrel and [4Fe–4S] cluster domains

Structures of bacterial MutY proteins show a catalytic domain and a C-terminal domain connected by a linker region.[41,42] The catalytic domain consists of the six-helix barrel and [4Fe–4S] cluster domains, while the C-terminal domain has structural similarity to MutT[43,44] and plays an important role in the recognition of 8-oxoG lesions.[43,45,46] Overall, hMYH shares a moderate amount of sequence identity with bacterial MutY proteins: 37% with EcMutY and 33.6% with *Bacillus stearothermophilus* MutY (BstMutY). Upon closer examination, sequence alignments indicate that the catalytic and C-terminal domains of hMYH and SpMyh1 share significant homology with the equivalent domains of EcMutY and BstMutY. In contrast, the IDC between the two domains of eukaryotic MYHs diverges significantly in sequence and length from bacterial MutY linkers. Such a marked change in an otherwise well-conserved homologue suggests a distinct role for the eukaryotic IDC in MYH function. In an attempt to visualize structural differences between the bacterial MutY linkers and the hMYH IDC, we crystallized a construct containing the catalytic domain (residues 65–292) and the IDC (residues 293–350) of hMYH (the full-length protein is 535 residues). The 31.7-kDa hMYH(65–350) protein contains the binding domains for 9-1-1 (residues 295–350 of hMYH),[39] APE1 (residues 293–318 of hMYH),[22] and hMSH6 (residues 232–254 of hMYH).[24] As the catalytic core of EcMutY is sufficient on its own to preserve glycosylase activity,[42] we confirmed that hMYH(65–350) maintains adenine glycosylase activity with DNA containing an A/8-oxoG mispair (Fig. S1).

The crystal structure of hMYH(65–350) was determined at 2.3 Å resolution using a combination of single-wavelength anomalous diffraction and molecular replacement for phasing (Fig. 1 and Table 1). The final model of hMYH(65–350) contains 271 residues for the first monomer in the asymmetric unit and 272 residues for the second monomer. Residues 65–67, 310–314, and 344–350 for monomer 1 (residues 65–67, 311–314, and 344–350 for monomer 2) are not visible in the electron density and therefore are not included in the final model. As expected, the structure of the catalytic domain of hMYH(65–350) is similar to that of EcMutY[42] (RMSD = 1.5 Å^2, 207 C^α residues; Fig. 1). Two α-helical domains comprise the catalytic domain: (1) a six-helix barrel domain composed of α helices α2–α7, and (2) a [4Fe–4S] cluster domain composed of α helices α1 and α8–α11 surrounding an [4Fe–4S] cluster. The six-helix barrel domain contains the helix–hairpin–helix (HhH) motif (α6–α7) including the hairpin residues L198, P199, G200, V201, and G202, which are also conserved in bacterial MutY enzymes.[42] Similar to the MutY enzymes, the HhH motif in hMYH is followed by a glycine-rich domain and a catalytically essential aspartate (D222). The [4Fe–4S] cluster domain contains four cysteine residues (C276, C283, C286, and C292) that ligand the [4Fe–4S] cluster. Corresponding cysteine residues in EcMutY and BstMutY exist, and the [4Fe–4S] cluster of hMYH is superimposable with the [4Fe–4S] clusters of these bacterial MutY enzymes. Also, based on structure-based sequence alignments with EcMutY and BstMutY, the hMYH residues 266-QAAME-270 of α10 and 120-EVMLQATA-127 of α3 are predicted to interact with adenine as part of the adenine specificity pocket at the interface between the six-helix barrel domain and the [4Fe–4S] cluster domain. Of the 13 BstMutY residues that contact the adenine nucleobase,[47] 11 are invariant; the exceptions are E188 (Q266 in hMYH) and I191 (M269 in hMYH).

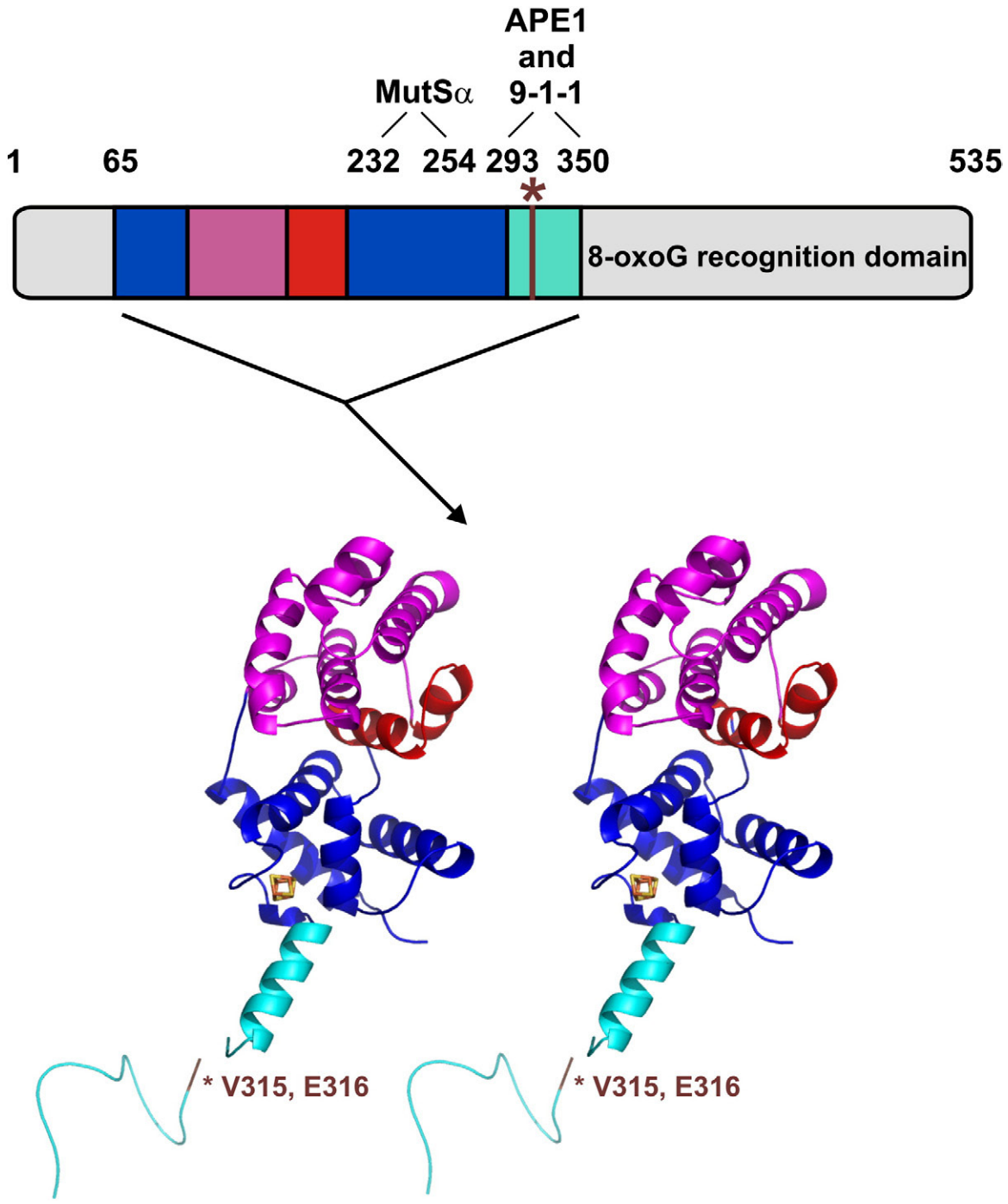

Fig. 1. Domain architecture of the catalytic domain (composed of the six-helix barrel and [4Fe–4S] cluster domains) and the IDC of hMYH. Stereo diagram of hMYH(65–350) including the six-helix barrel domain (magenta and red) with the signature HhH element (red) found in HhH GPD superfamily members. Cysteine residues of the [4Fe–4S] cluster domain (blue) coordinate the iron (orange) and sulfur (yellow) atoms of the [4Fe–4S] cluster. The IDC (cyan) connects the N-terminal catalytic domain to the C-terminal 8-oxoG recognition domain (not included in this structure). Residues V315 and E316 (brown) of hMYH are indicated (*) and correspond to residues I261 and E262 of SpMyh1. The schematic above the stereo diagram depicts the full-length hMYH protein and is color coded as described above to show the elements that compose the hMYH(65–350) crystal structure. The line in the schematic (*brown) also represents residues V315 and E316 of hMYH. The residues of hMYH that interact with MutSα (residues 232–254), APE1 (residues 293–318), and 9-1-1 (residues 295–350) are indicated above the schematic. Please note that other experiments in this work were conducted with SpMyh1 and that the 9-1-1 binding site consists of residues 245–293 of SpMyh1.

Table 1. Data collection and refinement statistics

	hMYH(65–350)
Data collection	
Space group	$P2_1$
Cell dimensions	
a, *b*, *c* (Å)	60.31, 82.17, 63.46
α, β, γ (°)	90, 100.9, 90
Resolution (Å)	2.3
R_{sym}	0.097 (0.437)[a]
$I/\sigma I$	18.7 (4.6)
Completeness (%)	95.8 (93.4)
Redundancy	7.6 (7.8)
Refinement	
Resolution (Å)	2.3
Number of reflections	24,674
R_{work}/R_{free}	20.6/25.1
Number of atoms	4225
Protein	4150
Ligand/ion	19
Water	56
B-factors	
Protein	66.165
Ligand/ion	63.634
Water	65.734
RMSD	
Bond lengths (Å)	0.017
Bond angles (°)	1.991

One crystal was used for the hMYH(65–350) structure.
[a] Values in parentheses are for the highest-resolution shell.

Despite the many structural similarities existing between hMYH and the bacterial MutY enzymes, some minor and major differences were evident. In the EcMutY structure and in the DNA-bound BstMutY structure, helix α1 of the [4Fe–4s] cluster domain begins at residues 3 and 9, respectively, while the corresponding helix α1 of hMYH(65–350) begins at residue 76. Residues 65–75 of hMYH exist in an extended conformation, and the structure and function of residues 1–64 of hMYH remain unknown. Nonetheless, residues 1–75 of hMYH account for additional structural domains that are not present in the bacterial MutY enzymes. Additionally, α1 of EcMutY is three residues shorter and angled slightly farther away from the globular center of the enzyme than α1 of hMYH(65–350). Another minor structural difference in hMYH(65–350) is observed at helices α2–α3. α2 of hMYH is longer than the corresponding helices in EcMutY and BstMutY by five and three residues, respectively, while α3 of hMYH is longer than the corresponding helices by four and three residues. The loop between α2 and α3 of hMYH is three residues long, while the corresponding loops in EcMutY and BstMutY are four and two residues long, respectively. Most of the structural differences in the catalytic domains of the hMYH and MutY enzymes are modest. The most significant differences exist in the hMYH IDC *versus* the bacterial MutY linkers, as described in detail below.

hMYH contains a unique IDC

The hMYH IDC (residues 292–353 of hMYH) is 41 residues longer than—and possesses little sequence homology with—the linker regions found in EcMutY (residues 208–228) and BstMutY (residues 214–234) (Fig. 2a). In the bacterial structures,[41,42] the short linker region extends only 5 Å away from the globular N-terminal catalytic domain before traversing a relatively direct path to the C-terminal 8-oxoG recognition domain. The MutY linker follows this path in both the apo-EcMutY structure and the BstMutY DNA structure, suggesting that there is no major conformational shift in the MutY linker upon binding to substrate DNA. Strikingly, the hMYH IDC consists of a short helical structure, α12 (Fig. 2b and c, cyan; Fig. S2), projecting 18.5 Å away from the catalytic domain (residues 293–305) before transitioning into an extended conformation. There are no crystal contacts that stabilize the helix itself, suggesting that the helical extension persists in the full-length protein. The orientation of α12 is stabilized by a covalent bond between residue C292 and the [4Fe–4S] cluster, plus nine hydrogen bonds among nearby residues (Fig. 2d), suggesting that the orientation observed in the hMYH(65–350) structure reflects that seen in the full-length protein. No visible density for residues 310–314 or residues 344–350 can be identified; however, residues 315–343 continue on a path away from the globular catalytic domain. Of functional significance, the structure of hMYH(65–350) shows that the proposed 9-1-1 binding region of hMYH (residues 295–350) is within the IDC, which projects away from the catalytic domain. In this position and conformation, the IDC would provide an ideal scaffold without structural obstacles to promote the interaction between hMYH and 9-1-1.

I261 and E262 of the SpMyh1 IDC are important mediators of the interaction with *S. pombe* 9-1-1

In SpMyh1, the IDC comprises residues 245–293. Using a glutathione *S*-transferase (GST) pull-down assay, we previously showed that mutation of I261 of the SpMyh1 IDC to alanine [SpMyh1(I261A)] attenuates its interaction with SpHus1.[39] Of the three 9-1-1 subunits, SpHus1 is the preferred binding partner of SpMyh1 and is therefore used in pull-down assays to estimate relative 9-1-1 binding proficiency. Because the I261A mutation resulted in partial disruption of the 9-1-1 interaction, we sought to further disrupt the interaction between SpHus1 and SpMyh1 by creating a mutation at E262, another highly conserved residue within the proposed Hus1 binding region of SpMyh1.[39] In addition, both I261 and E262 reside in the extended region that lies just beyond the helical structure of the IDC (equivalent to V315 and E316 of hMYH; Figs. 1 and 2a). Thus, we performed site-directed

mutagenesis of SpMyh1(I261A) to replace E262 with glutamine (E262→Q262). As predicted, the interaction between the SpMyh1(I261A/E262Q) mutant and SpHus1 is significantly weakened compared to the interaction between SpMyh1(I261A) and SpHus1 (Fig. 3a, lanes 3 and 4).

The purified SpMyh1(I261A/E262Q) mutant protein exhibits glycosylase activity with the A/8-oxoG substrate similar to those of the wild-type (WT) and SpMyh1(I261A) enzymes (Fig. 3b–d, lane 2). However, consistent with its weakened association with SpHus1, SpMyh1(I261A/E262Q) requires greater

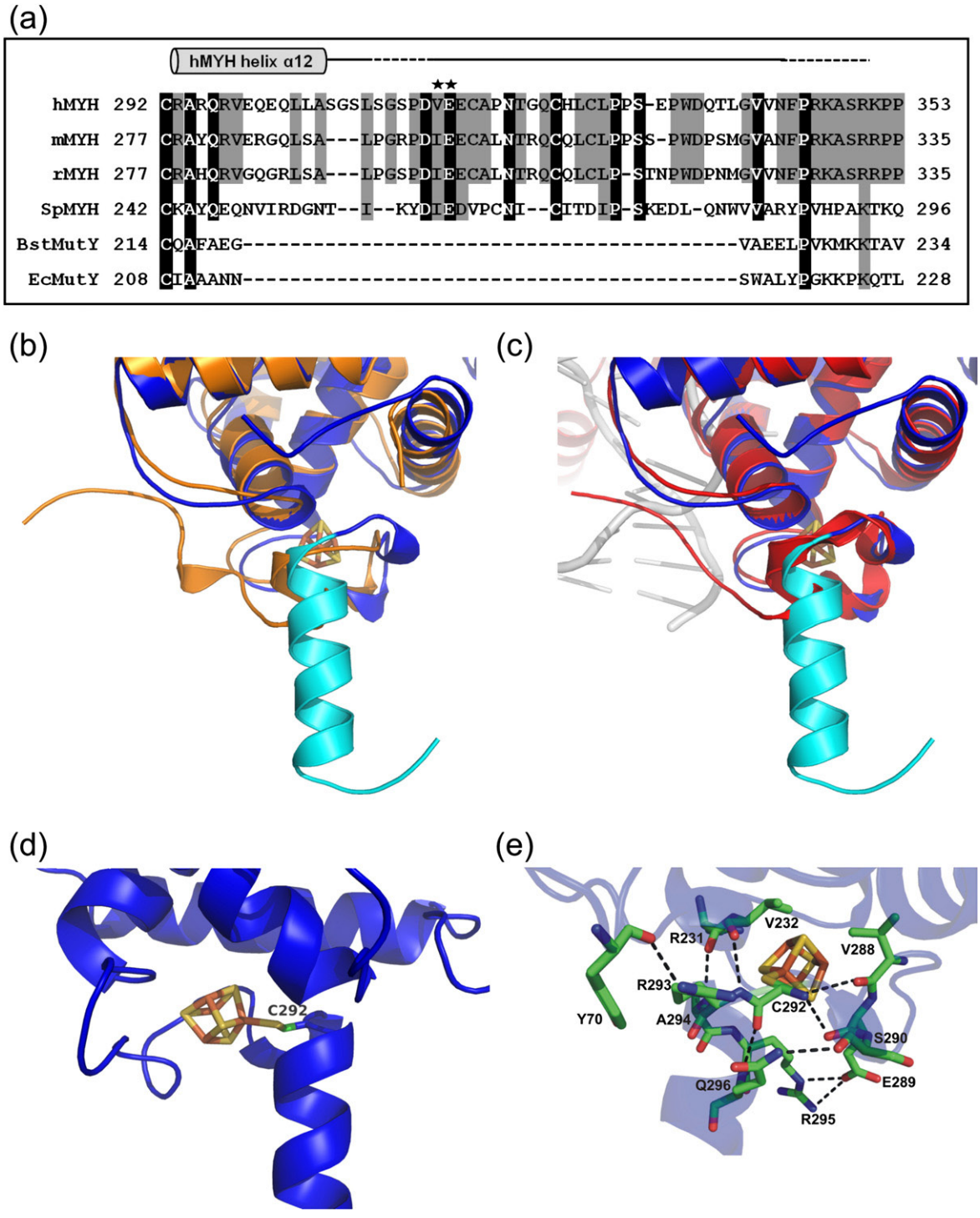

Fig. 2 *(legend on next page)*

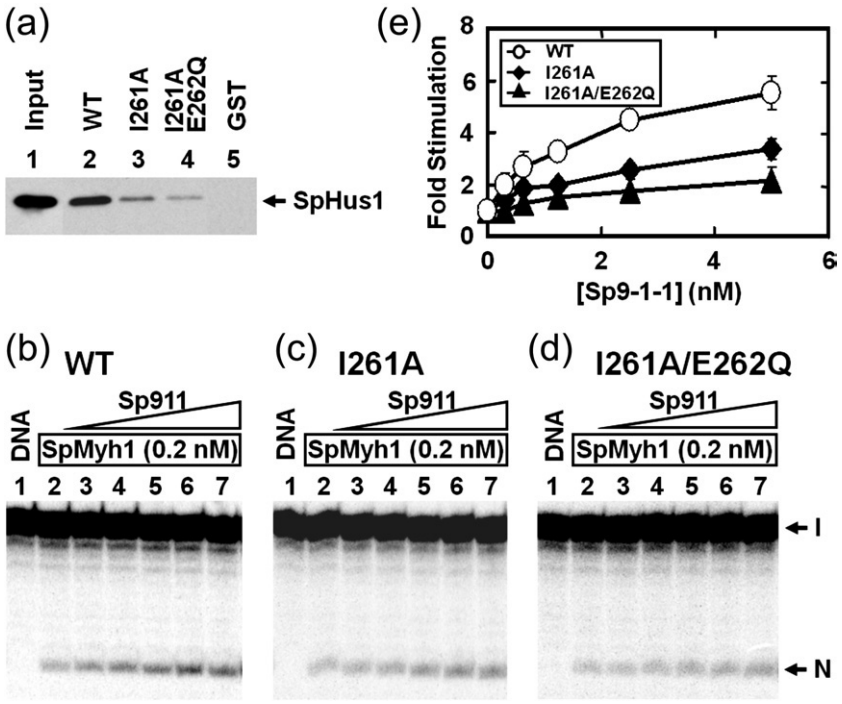

Fig. 3. I261 and E262 of SpMyh1 are important for 9-1-1 binding. (a) Physical interactions between SpHus1 and SpMyh1 mutants examined via a GST pull-down assay. Lane 1 contains 10% input of *E. coli* cell extracts containing His-SpHus1. Lanes 2–5 are pellets containing His-SpHus1 from *E. coli* cell extracts pulled down by GST-SpMyh1 (WT), GST-SpMyh1(I261A), GST-SpMyh1(I261A/E262Q), or GST alone, respectively. The pellets were fractionated on a 10% SDS-PAGE gel, and Western blot analysis was performed with anti-His_6 antibody. Equal amounts of GST and GST fusion proteins were immobilized onto glutathione-Sepharose 4B beads (data not shown). (b–d) *S. pombe* 9-1-1 complex stimulates the glycosylase activity of SpMyh1 mutants. Lane 1 of each panel represents DNA substrates containing A/8-oxoG. The DNA substrate (0.18 nM) was incubated with recombinant SpMyh1 (0.2 nM) (lane 2 of each panel). Lanes 3–7 are similar to lane 2, but with added 0.313 nM, 0.625 nM, 1.25 nM, 2.5 nM, and 5 nM *S. pombe* 9-1-1 complex purified from *E. coli*, respectively. Reactions were carried out at 30 °C for 30 min, and the products were separated on a 14% DNA sequencing gel. The gel images were viewed on a PhosphorImager and quantified using the ImageQuant software (GE Healthcare). Arrows mark the intact DNA substrate (I) and the nicked product (N). (e) Quantitative analyses of the fold stimulation of the *S. pombe* 9-1-1 complex on SpMyh1-WT (open circles), SpMyh1(I261A) (filled diamonds), and SpMyh1 (I261A/E262Q) (filled triangles). The area at the product position in the control lane (no protein; lane 1 of b–d) was subtracted as background signal. SpMyh1 cleavage activity was calculated by the percentages of nicked product over total DNA (product plus substrate bands). SpMyh1 glycosylase activities from three experiments are shown. Error bars represent the standard deviations of the means.

Fig. 2. The hMYH IDC projects away from the catalytic domain. (a) Structure-based sequence alignment of the linker regions of prokaryotic MutY proteins and the IDCs of eukaryotic species. The sequences are as follows: *Homo sapiens* MYH (hMYH; accession no. U63329), *Mus musculus* MYH (mMYH; accession no. AY007717), *Rattus norvegicus* MYH (rMYH; accession no. Q8R5G2), SpMyh1 (accession no. Z69240), BstMutY (accession no. 46015544), and EcMutY (accession no. P17802). Identical amino acid residues that are present in at least four sequences are boxed in black, and conserved residues are boxed in gray. The hMYH IDC includes the residues required for interaction with APE1 (residues 293–318 of hMYH) and Hus1 (residues 295–350 of hMYH). Stars indicate SpMyh1 residues I261 and E262, which are important for the 9-1-1 interaction. The gray cylinder above the sequence alignment depicts helix α12 of hMYH(65–350) at the beginning of the IDC. The following continuous line indicates additional residues of the IDC that are in an extended conformation. The portions of the line that are dotted indicate residues 310–314 and 344–350 for which no electron density was identified from the hMYH(65–350) crystal structure. (b and c) The hMYH structure is overlaid with the apo-EcMutY structure (b; orange) and the DNA-bound BstMutY structure (c; red) to highlight differences between the hMYH IDC and the bacterial MutY linkers. The hMYH IDC (b and c; cyan) projects 18.5 Å away from the catalytic domain, differing from the more direct paths of the bacterial MutY linkers to the C-terminal domain. In both the apo-EcMutY structure and the DNA-bound BstMutY structure, the linkers only extend 5 Å away from the catalytic domain. (d) The orientation of the hMYH IDC is stabilized by a covalent bond between residue C292 and the [4Fe–4S] cluster. (e) The orientation of the hMYH IDC is further stabilized by nine hydrogen bonds (black broken lines). The oxygen (red) and nitrogen (blue) atoms involved are shown. Importantly, some of these hydrogen bonds involve R231, V232, and R295, which are each associated with MAP mutations.

amounts of the *S. pombe* 9-1-1 complex (Fig. 3d and e) to increase its glycosylase activity to the same extent as that seen for SpMyh1-WT (Fig. 3b and e). Two-fold stimulation of SpMyh1-WT (0.2 nM) requires a slight molar excess of *S. pombe* 9-1-1 (0.3 nM), but a 25-fold molar excess of *S. pombe* 9-1-1 (5 nM) is needed for 2-fold stimulation of SpMyh1 (I261A/E262Q) (Fig. 3e). At a concentration of 5 nM, the *S. pombe* 9-1-1 complex stimulates the glycosylase activities of SpMyh1-WT, SpMyh1(I261A), and SpMyh1(I261A/E262Q) by approximately 5.5-fold, 3.3-fold, and 2.1-fold, respectively (Fig. 3e).

Expression of the I261A/E262Q IDC mutant of SpMyh1 in *myh1*Δ cells confers a mutator phenotype

We have shown that the *S. pombe myh1*Δ strain displays a mutator phenotype[8] (Table 2, line 2) and that expression of SpMyh1-WT in these cells reduces the mutation frequency to the same level as WT cells (Table 2, line 3). To test whether interaction with the 9-1-1 complex is important for *in vivo* SpMyh1 function, we examined the mutation frequency of JSP303-Y4 (*myh1*Δ) yeast cells expressing the SpMyh1(I261A/E262Q) mutant. The expression level of SpMyh1(I261A/E262Q) protein in yeast cells is comparable to that of SpMyh1-WT under the same conditions (data not shown). The mutation frequency of *myh1*Δ yeast cells expressing the SpMyh1(I261A/E262Q) mutant is 28-fold higher than that of the WT strain (Table 2, compare line 4 to line 1) ($P=0.003$) and is 2-fold lower than that of the parental *myh1*Δ strain (Table 2, compare line 4 to line 2) ($P=0.05$). Thus, the SpMyh1(I261A/E262Q) mutant cannot complement chromosomal *myh1* deletion. These results provide direct evidence that the interaction between SpMyh1 and the *S. pombe* 9-1-1 complex is important to maintain the SpMyh1 biological function of mutation avoidance.

A peptide consisting of the SpMyh1 IDC (residues 245–293) interacts with the 9-1-1 complex

Using deletion constructs, we have previously shown that residues 245–293 of SpMyh1 are required for 9-1-1 binding.[39] To further demonstrate that these residues associate with 9-1-1, we expressed His-tagged and green fluorescence protein (GFP)-tagged SpMyh1(245–293) using plasmids pRep41X and p4XG, respectively. Expression of the SpMyh1(245–293) peptide is demonstrated by Western blot analysis (Fig. 4a, lane 2; Fig. 4c, lane 1). Because the *nmt1* promoter controls the transcription of cDNA in pREP41X and p4XG, SpMyh1(245–293) expression is regulated by varying the concentrations of thiamine (vitamin B1) used in minimal media during the growth of yeast cells. At 5 μg/ml thiamine, expression of the His-tagged and GFP-tagged peptides is almost completely suppressed (Fig. 4a, lane 3; Fig. 4c, lane 2).

Table 2. Mutation frequencies of *S. pombe* strains

Strain	Mutation frequency ($FOA^R/10^8$ cells)	Fold
1. JSP303 (WT)	3.3±2.4[a]	1
2. *myh1*Δ	167±40[a]	50
3. *myh1*Δ+SpMyh1-WT	7.4±1.9[a]	2
4. *myh1*Δ+SpMyh1(I261A/E262Q)	95±12	28

The superscripted "R" denotes resistance to the normally toxic FOA.

[a] The values (mean+standard deviation) in this study are comparable to those derived from Chang *et al.*[8]

The association between the SpMyh1(245–293) peptide and the 9-1-1 proteins was examined with GST pull-down assays. GST-tagged hHus1, hRad1, and hRad9 proteins were immobilized on three separate bead preparations and used to pull down His-tagged SpMyh1(245–293) peptide from yeast extracts. As shown in Fig. 4b, the SpMyh1(245–293) peptide binds to GST-hHus1 (lane 2) and GST-hRad1 (lane 3). However, the same peptide cannot bind to GST-Rad9 (lane 4), which displays a binding level similar to the negative control of GST alone (lane 5). Thus, the SpMyh1(245–293) peptide binds to the 9-1-1 complex asymmetrically. The weak binding of SpRad9 to the peptide is consistent with our published data indicating that Rad9 is the weakest binding partner of the 9-1-1 complex subunits for both intact SpMyh1 and hMYH.[38,39] As a result, we named the SpMyh1(245–293) peptide SpHIP (*SpH*us1-*i*nteracting *p*eptide).

The interaction of SpHIP with the 9-1-1 complex was also demonstrated by coimmunoprecipitation. GFP-tagged SpHIP was expressed in the Hus1-MYC strain of *S. pombe* cells, which expresses Myc-tagged SpHus1 (Table S1, line 3). The GFP antibody was used to precipitate the GFP-tagged SpHIP from cell extracts. The SpHus1 protein is coprecipitated with GFP-tagged SpHIP (Fig. 4d, lane 3), but not with GFP alone (Fig. 4d, lane 6), indicating that SpHIP can interact with 9-1-1 *in vivo*. Finally, we tested whether SpHIP interferes with SpMyh1–SpHus1 interaction. Increasing amounts of yeast extracts containing SpHIP were added to the GST pull-down reactions with immobilized GST-SpHus1 and purified SpMyh1. As shown in Fig. 4e, His-tagged SpHIP inhibits the interaction between SpHus1 and SpMyh1.

Expression of SpHIP renders *S. pombe* cells more sensitive to H_2O_2

To further study the interaction between SpMyh1 and 9-1-1 *in vivo*, we expressed SpHIP in *S. pombe* cells and analyzed its influence on H_2O_2 sensitivity. *S. pombe* cells were transfected with a plasmid

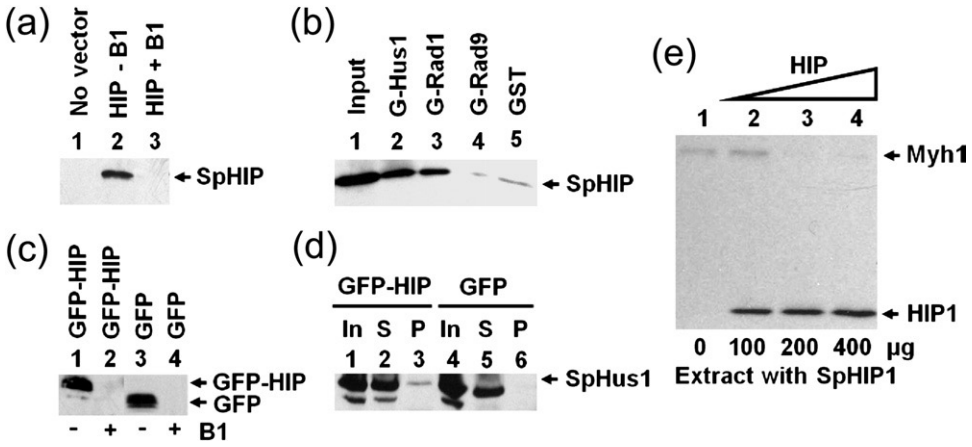

Fig. 4. (a) Expression of a His-tagged SpHIP peptide derived from residues 245–293 of SpMyh1 in *S. pombe*. Equal protein amounts were loaded on a 20% SDS-PAGE gel, and Western blot analysis was performed with antibody against SpMyh1. Lane 1, extract from *myh1*Δ yeast cells; lane 2, extract from *myh1*Δ cells expressing the His-tagged SpHIP peptide in the absence of thiamine (B1); lane 3, similar to lane 2, except that the His-tagged SpHIP peptide is not expressed in the presence of 5 μg/ml thiamine. (b) Interaction of SpHus1, SpRad1, and SpRad9 with His-tagged SpHIP. *S. pombe* cells were transfected with a plasmid containing the His-tagged SpHIP peptide derived from residues 245–293 of SpMyh1. Extracts derived from these yeast cells were incubated with GST-SpHus1, GST-SpRad1, or GST-SpRad9 immobilized on beads to observe the binding interactions between SpHIP and the 9-1-1 complex components. Equal amounts of GST and GST fusion proteins were loaded (data not shown). His-tagged SpHIP in the pellets was detected by Western blot analysis using anti-SpMyh1 antibody. (c) Expression of a GFP-tagged SpHIP peptide derived from residues 245–293 of SpMyh1 in Hus1-MYC *S. pombe* cells. Lane 1, extract from Hus1-MYC cells expressing GFP-SpHIP in the absence of thiamine (B1); lane 2, similar to lane 1, except that GFP-SpHIP is not expressed in the presence of 5 μg/ml thiamine; lane 3, extract from Hus1-MYC cells expressing GFP in the absence of thiamine; lane 4, similar to lane 3, except that GFP is not expressed in the presence of 5 μg/ml thiamine. (d) Coimmunoprecipitation of SpHus1 with GFP-SpHIP by anti-GFP antibody. *S. pombe* cells containing Myc-tagged SpHus1 were transfected with a plasmid containing GFP-SpHIP or GFP alone. Immunoprecipitation was performed with anti-GFP antibody, and Western blot analysis was detected by anti-Myc antibody. S and P represent supernatant and pellet, respectively. (e) SpHIP inhibits SpMyh1–SpHus1 interaction. Lane 1, purified SpMyh1 (0.1 μg) was incubated with GST-SpHus1 immobilized on beads; lanes 2–4, increasing amounts of extracts containing SpHIP (as indicated) were added to reactions with immobilized GST-SpHus1 and purified SpMyh1, similar to lane 1. Both SpMyh1 and SpHIP were detected in the pellets by Western blot analysis using anti-SpMyh1 antibody.

containing GFP-SpHIP and grown in minimal media with or without 5 μg/ml thiamine. At H_2O_2 concentrations higher than 1.5 mM, expression of SpHIP markedly increases H_2O_2 sensitivity (Fig. 5, gray bars) compared with cells not expressing SpHIP (Fig. 5, white bars). The expression of GFP-SpHIP alone does not affect the growth rate of *S. pombe* cells (data not shown).

The SpMyh1 IDC is required to promote DNA damage selection and robust glycosylase activity of the eukaryotic enzyme

In order to further examine the functional impact of differences between the linker regions of prokaryotic MutY proteins and the IDCs of eukaryotic MYH proteins, we constructed an SpMyh1–EcMutY Chimera (SpMyh1-Chimera), which contains the N-terminal domain (residues 1–244) and the C-terminal domain (residues 289–461) of SpMyh1 connected by the shorter linker region (residues 214–227) of EcMutY (Fig. 6a). The SpMyh1-Chimera was designed to maintain the N-terminal catalytic domain and the C-terminal 8-oxoG recognition domain of the glycosylase while eliminating the 9-1-1 interaction domain found only in eukaryotic MYH proteins. We designed this construct in such a manner to ensure that the chimeric linker is long enough to traverse the DNA and to allow SpMyh1-Chimera to encircle it, as is required for high-affinity binding.[41,48,49] As a preliminary check on our design, we used SWISS-MODEL[50] to create a homology model of the SpMyh1-Chimera (Fig. S3); in the model, the linker appears to be of sufficient length to allow the C-terminal domain to access the 8-oxoG lesion. In addition, the observed affinity of SpMyh1-Chimera for abasic product DNA (see the text below) indicates that the *E. coli* linker in the context of the SpMyh1-Chimera is long enough to position the SpMyh1 C-terminal domain on the lesion side of the DNA.

We compared the glycosylase activity of SpMyh1-Chimera to that of the WT enzyme to assess SpMyh1-Chimera as a functional glycosylase. For an accurate comparison, both SpMyh1-Chimera and SpMyh1-WT were expressed with the same maltose-

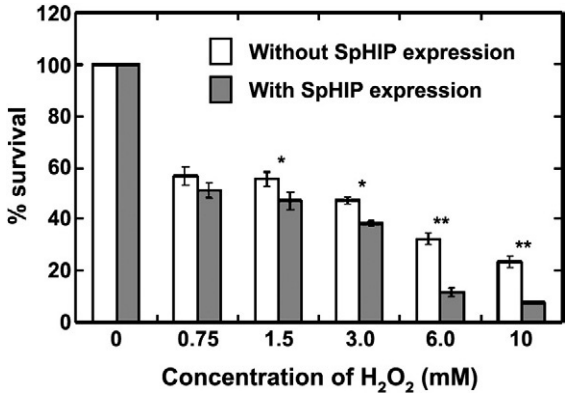

Fig. 5. H_2O_2 sensitivity of *S. pombe* cells expressing GFP-SpHIP. *S. pombe* BM2681 cells were transfected with a plasmid containing GFP-SpHIP and grown in minimal medium with or without 5 μg/ml thiamine. The expression of GFP-SpHIP is inhibited with thiamine. Cells were treated with H_2O_2 for 30 min and recovered in fresh media without H_2O_2 for an additional 2 h. The percentages of surviving cells after H_2O_2 treatment were measured. At H_2O_2 concentrations higher than 1.5 mM, expression of SpHIP increased H_2O_2 sensitivity compared with cells not expressing SpHIP. For cells exposed to H_2O_2 concentrations of 1.5 mM and 3.0 mM, the increased sensitivities measured were statistically significant at $^*P<0.02$. For cells exposed to H_2O_2 concentrations of 6.0 mM and 10.0 mM, the increased sensitivities measured were statistically significant at $^{**}P<0.001$.

binding protein (MBP) affinity tag and purified using similar protocols. As shown in Fig. 6b, while SpMyh1-WT has robust glycosylase activity (at a concentration of 26 nM) with A/8-oxoG-containing DNA, no enzymatic activity is observed for SpMyh1-Chimera at the same concentration. At a 10-fold increase in protein concentration (260 nM), SpMyh1-Chimera displays only minimal enzymatic activity. At 2600 nM, SpMyh1-Chimera shows increased enzymatic activity, but still not at a level equal to that of SpMyh1-WT at 26 nM. Although the enzymatic activity of SpMyh1-Chimera is not completely abolished, it is markedly reduced compared to that of SpMyh1-WT.

To investigate the potential cause of the reduced enzymatic activity of SpMyh1-Chimera, we compared the DNA binding affinities of SpMyh1-Chimera *versus* SpMyh1-WT using fluorescence anisotropy experiments. We incubated a fluorescein-labeled 20-bp duplex DNA containing the product of the SpMyh1 glycosylase reaction (an AP/8-oxoG mispair) with either SpMyh1-Chimera or SpMyh1-WT over a range of protein concentrations (Fig. 6c). Binding isotherms were fitted for each protein using a transformed Hill equation (see Materials and Methods), which yields a parameter ($[P]_{1/2}$) that approximates the protein concentrations at which half maximal binding is achieved. Unexpectedly, the SpMyh1-Chimera and SpMyh1-WT proteins have very similar affinities for the DNA substrate containing an AP/8-oxoG mispair, with half maximal binding at 12±3 nM and 10±2 nM, respectively. Both proteins display apparent binding cooperativity with Hill coefficients of 2.6±1.1 and 3.7±1.1 for SpMyh1-Chimera and SpMyh1-WT, respectively.

To clarify the DNA substrate preference of SpMyh1-Chimera, we performed a competition assay. We compared the abilities of unlabeled substrates containing either a C:G pair or an A/8-oxoG mispair to displace a fluorescein-labeled A/8-oxoG substrate bound to SpMyh1-Chimera or SpMyh1-WT. As expected, the unlabeled A/8-oxoG substrate (Fig. 6d, black circles) can displace the fluorescein-labeled A/8-oxoG substrate bound

Fig. 6. The SpMyh1 linker domain is important for DNA damage specificity and glycosylase activity. (a) Schematic depicting the SpMyh1-Chimera protein. The SpMyh1-Chimera is composed of the N-terminal and C-terminal domains of SpMyh1 (residues 1–244 and 289–461 of SpMyh1) connected by the EcMutY linker (residues 214–227 of EcMutY). (b) Glycosylase activity of SpMyh1-Chimera. Lane 1, DNA substrate (0.18 nM) containing A/8-oxoG; lane 2, the DNA substrate incubated with SpMyh1-WT (26 nM); lanes 3–5, the DNA substrate incubated with increasing concentrations of SpMyh1-Chimera (26 nM, 260 nM, and 2600 nM, respectively). Reactions were carried out for SpMyh1-WT and SpMyh1-Chimera at 30 °C and 25 °C, respectively, for 60 min. The products were separated on a 14% DNA sequencing gel, and the gel image was viewed on a PhosphorImager. Arrows mark the intact DNA substrate (I) and the nicked product (N). Although SpMyh1-WT has robust enzymatic activity at a concentration of 26 nM, no glycosylase activity was observed for SpMyh1-Chimera at the same concentration. At 10-fold and 100-fold increases in protein concentration (260 nM and 2600 nM, respectively), SpMyh1-Chimera has some glycosylase activity but not at a level equal to that of SpMyh1-WT. (c) Abasic DNA product affinities of SpMyh1-WT and SpMyh1-Chimera. A fluorescein-labeled 20-bp duplex DNA with a centrally located 8-oxoG base opposite an abasic site was incubated with either SpMyh1-WT or SpMyh1-Chimera over a range of protein concentrations. Binding isotherms were fitted for each protein, and the relative affinities for the substrate DNA were approximated based on the calculated midpoint concentrations. (d) DNA substrate specificity of SpMyh1-Chimera. Reactions were preincubated with 150 nM SpMyh1-Chimera or SpMyh1-WT, 1 nM fluorescein-labeled 20-bp duplex DNA with a centrally located A/8-oxoG mispair, and unlabeled competitor substrates (with a centrally located A/8-oxoG mispair or C:G pair) over a range of concentrations (0–1000 nM) at room temperature for 30 min. The unlabeled A/8-oxoG substrate (black circles) can displace the fluorescein-labeled A/8-oxoG substrate bound to SpMyh1-Chimera or SpMyh1-WT. The unlabeled C:G substrate can displace the fluorescein-labeled A/8-oxoG substrate bound to SpMyh1-Chimera (right; red diamonds) but not SpMyh1-WT (left; red diamonds).

to SpMyh1-Chimera or SpMyh1-WT with measured apparent inhibition constants ($K_{i,app}$) of 42±9 nM and 14±9 nM, respectively. Thus, the competition assay indicates that the SpMyh1-Chimera binds an A/8-oxoG DNA with less affinity than the WT protein. However, the C:G substrate is an ineffective competitor for SpMyh1-WT and is unable to displace the fluorescein-labeled A/8-oxoG substrate to any measurable extent (Fig. 6d, left, red diamonds). Strikingly, the C:G substrate can displace the fluorescein-labeled A/8-oxoG substrate bound to SpMyh1-Chimera ($K_{i,app}$ = 17±4 nM) (Fig. 6d, right, red diamonds) and is therefore an effective competitor. In addition, upon measurement of direct binding to fluorescein-labeled 20-bp C:G substrate, SpMyh1-Chimera binds the substrate with high affinity, whereas SpMyh1-WT does not bind the substrate to any measurable extent (Fig. S4). These results indicate that SpMyh1-Chimera exhibits only a modest preference for binding A/8-oxoG-containing DNA relative to undamaged DNA.

Discussion

In this study, we solved the first eukaryotic MYH structure and examined the significance of the interaction between MYH and the 9-1-1 complex for the promotion of DNA repair. Our studies provide a structural rationale for the additional

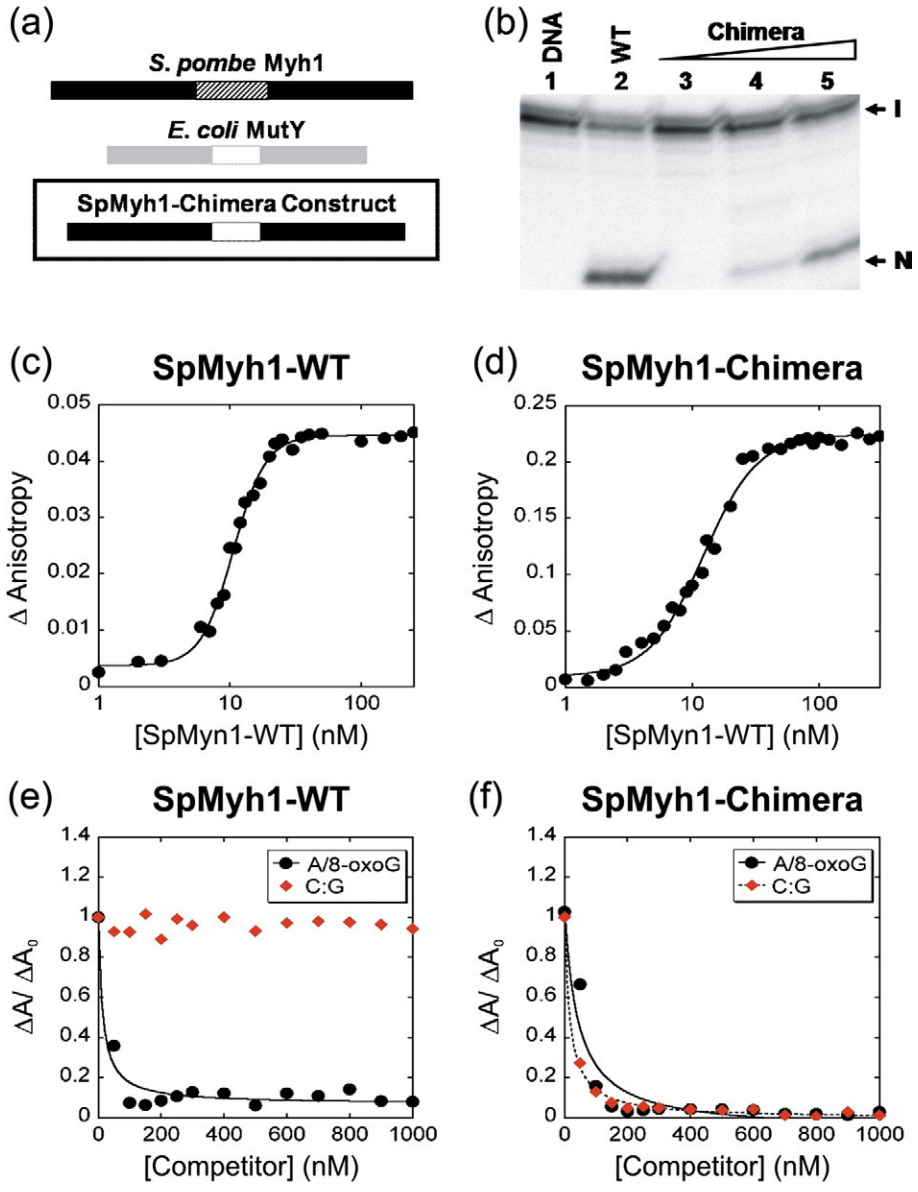

Fig. 6 *(legend on previous page)*

residues found in eukaryotic MYH IDCs. We have demonstrated that two residues of SpMyh1 (I261 and E262), which reside on the extended region of the IDC, are key mediators of the interaction between SpMyh1 and 9-1-1. Importantly, disruption of the interaction between SpMyh1 and the 9-1-1 complex via mutation [SpMyh1(I261A/E262Q)] has a deleterious impact on oxidative DNA repair *in vivo*. When the IDC of SpMyh1 is replaced by the EcMutY linker, the protein binds abasic product DNA with normal affinity, but also binds undamaged DNA with abnormally high affinity, resulting in substantially abrogated glycosylase activity. Thus, the IDC of eukaryotic MYH serves as a structural scaffold to mediate important protein interactions and simultaneously serves as a structural hinge to properly position the N-terminal and C-terminal domains for A/8-oxoG recognition and catalysis.

Transient interactions between hMYH and other proteins coordinate MYH BER with DNA replication, other DNA repair pathways, and DNA damage response.[6] At a basic level, these interactions may promote the efficient transfer of the product of one step of repair to the next enzyme in the repair pathway. At first glance, the effects of these interactions appear minor, as the catalytic activity of MYH increases only 5-fold, at best, in the presence of a high excess of a given stimulatory protein. However, upon closer inspection, the observed effects seem to primarily foster cycling through the BER pathway and, if necessary, transitioning to other processes. This "BER relay" system appears to operate at the expense of maximizing the catalytic turnover of any particular enzyme. Such a regulatory network of malleable protein interactions affords the BER pathway sufficient flexibility to repair multiple types of damage. In that regard, high-affinity interactions between MYH and interacting proteins are likely not optimal for the seamless incorporation of MYH BER into other pathways of DNA metabolism.

Thus far, a partial sketch of this protein interaction regulatory network has been assembled through a systematic pairwise investigation of the effects of interacting partners on MYH activity. APE1, a downstream BER enzyme, interacts with MYH[22] and enhances its glycosylase activity.[51] This interaction likely promotes MYH turnover and prevents the release of potentially cytotoxic AP sites. MYH activity can be also stimulated by the mismatch recognition protein MSH2/MSH6 (MutSα).[24] In particular, the repair of A/8-oxoG mispairs requires communication between the BER pathway and the mismatch repair pathway and coupling to DNA replication[21–25] to ensure that the misincorporated adenine on daughter strand DNA—rather than 8-oxoG on parental strand DNA—is repaired. Finally, MYH interacts with 9-1-1, resulting in an increase in MYH glycosylase activity.[38,39] The interaction with 9-1-1 is enhanced by stresses such as H_2O_2 and ionizing radiation exposure,[38,39] consistent with the suggestion that 9-1-1 might replace PCNA under stress[52] to arrest the cell cycle and to simultaneously enhance BER.

Our hMYH(65–350) crystal structure further supports the idea that transient protein interactions regulate the activity of hMYH. While the hMYH IDC is required to maintain a physical link to the 9-1-1 complex and to APE1, the structure of hMYH(65–350) reveals that the hMYH IDC possesses no regular secondary or tertiary structure beyond the helical extension (residues 293–305; Figs. 1 and 2b–d). Interestingly, the 9-1-1 interacting regions of other DNA glycosylases, including hNEIL1 (residues 290–350)[53] and hTDG (residues 67–110),[54] may also be flexible. No identifiable density beyond residue 290 can be detected in the crystal structure of hNEIL1 containing residues 2–343.[53] Similarly, NMR data indicate that residues 67–110 of hTDG are unstructured. Thus, a common feature of the 9-1-1 binding motif appears to be that it adopts a flexible structure, possibly to enable transient interactions with multiple protein partners. Still, it is possible that this region becomes more structured in the presence of the 9-1-1 complex, resulting in a conformational change that promotes the catalytic activities of DNA glycosylases. Of note, it has been observed that many unstructured protein segments do not fold until they bind to their biological targets, thus permitting protein promiscuity.[55]

Structure-based sequence alignment shows that the IDCs of hMYH and SpMyh1 are 41 and 34 residues longer, respectively, than the linker of the bacterial MutY proteins (Fig. 2a). Eukaryotic MYH family members possess few conserved stretches within their IDCs, with only an ~25% sequence identity between the hMYH IDC and the SpMyh1 IDC. Our hMYH(65–350) structure provides a potential rationale for the added length of the IDC. The additional length of the hMYH IDC appears to serve, in part, to project the 9-1-1 interacting region away from the surface of bound DNA (Fig. S5). Without projection of the IDC away from the catalytic domain and the DNA binding site, the modest features of the IDC might be obscured by the negative charge of DNA and thus prevent the interaction between MYH and the 9-1-1 complex. The orientation of the hMYH IDC is stabilized by the covalent bond between residue C292 and the [4Fe–4S] cluster, plus nine additional hydrogen bonds (Fig. 2d). Any significant reorientation of the IDC would require accommodation of hydrogen-bonding groups without exposure of the [4Fe–4S] cluster to solvent, a further indication that the orientation we observe is likely fixed. Significantly, some of these hydrogen bonds involve residues R231, V232, and R295, each of which has an

associated MAP mutation.[14] Additionally, residues R295, Q324, F344, and P345 of hMYH are all within the IDC and are associated with MAP mutations[14] (Fig. 2a). It will be interesting to see whether any newly discovered MAP mutations will include mutations that disrupt the interaction between hMYH and 9-1-1.

Although the interaction between MYH and 9-1-1 produces a modest effect on catalytic activity *in vitro*, the interaction is still of great physiological significance. In previous studies,[39] we showed that mutation of I261 to alanine alone could attenuate the interaction between SpMyh1 and 9-1-1 without perturbing catalytic activity. However, the effect was modest. We demonstrated here that the interaction with 9-1-1 is more severely compromised for the SpMyh1(I261A/E262Q) mutant than for the SpMyh1(I261A) mutant (Fig. 3). This allowed us to assess the impact of the disruption of the SpMyh1/9-1-1 interaction on oxidative DNA damage repair *in vivo*. Unlike SpMyh1-WT, SpMyh1(I261A/E262Q) does not reduce the mutation frequency of *myh1*Δ cells (Table 2). In a separate approach, we showed that disruption of the interaction between MYH and 9-1-1 in *S. pombe* cells through expression of SpHIP (Fig. 4) makes cells more sensitive to H_2O_2 (Fig. 5), reducing the DNA repair capacity of the cells. Since the IDC of hMYH also contains the human APE1 binding site (residues 295–318),[22] it is possible that SpHIP may also interfere with the interaction between SpMyh1 and APE1.

By making more radical changes to the IDC, we demonstrate that its impact extends beyond mediating protein interactions. We created a chimeric protein that replaced the region of the SpMyh1 IDC implicated in 9-1-1 interactions with the EcMutY linker in an attempt to retain catalytic activity while abolishing 9-1-1 interactions. However, characterization of SpMyh1-Chimera reveals that the eukaryotic IDC is designed not only to promote protein–protein interactions but also to foster substrate selection and catalytic activity (Fig. 6). Despite the preservation of the catalytic and C-terminal domains (Fig. 6a), the SpMyh1-Chimera has significantly reduced glycosylase activity (Fig. 6b). In contrast, the SpMyh1-Chimera maintains normal affinity for the abasic DNA product (Fig. 6c). Such high-affinity binding requires extensive interactions between both N-terminal and C-terminal domains and the bound DNA. In particular, the isolated N-terminal domains of both EcMutY[48] and hMYH (E.A.T., unpublished) exhibit a marked reduction in affinity for the abasic product. Furthermore, the isolated EcMutY C-terminal domain has no intrinsic affinity for DNA.[56] Thus, high-affinity binding requires successful positioning of both domains simultaneously on DNA. If the creation of the SpMyh1-Chimera retains WT abasic product affinity, some deficit in substrate recognition must explain the severe catalytic defect. In fact, our data show that the SpMyh1-Chimera binds undamaged DNA with abnormally high affinity (Fig. 6d; Fig. S4). This gain of function (i.e., nonspecific DNA binding) relative to the WT enzyme was unexpected and suggests an active role for the IDC in promoting catalysis. It appears that the extra length of the IDC might be required to properly orient the catalytic and C-terminal domains on substrate DNA to optimize the contacts required for preferential binding to an A/8-oxoG mispair. The fact that the SpMyh1-Chimera poorly catalyzes the glycosylase reaction with the radical change in DNA binding behavior suggests that the process of encountering the lesion might be impaired. In effect, the SpMyh1-Chimera might spend far more time engaged with undamaged DNA than the WT enzyme and, perhaps as a result, only infrequently recognizes A/8-oxoG mispairs. These data provide an additional potential explanation for the presence of large insertions (41 residues in hMYH and 34 residues in SpMyh1) in eukaryotic IDCs. The IDCs provide an accessible platform for protein–protein interactions while retaining the ability to help orient the N-terminal and C-terminal domains for catalysis. Satisfying these simultaneous constraints likely necessitated the large insertions observed in eukaryotic IDCs rather than the more modest changes observed in the N-terminal and C-terminal domains.

Here we demonstrate for the first time that the eukaryotic MYH IDC is not merely an inert tether that connects the catalytic and C-terminal 8-oxoG recognition domains but rather is essential for the *in vitro* and *in vivo* functions of MYH. Our work provides insight into how protein interactions of modest affinity, such as that between MYH and 9-1-1, can modulate BER and play an important role in mutation avoidance. Even slight changes to the MYH IDC can diminish the ability of the enzyme to mitigate the mutagenic potential of oxidative DNA damage *in vivo.* Despite relatively modest structural differences between eukaryotic IDCs and prokaryotic linker regions, the hMYH IDC provides an ideal "docking station" for 9-1-1 (and APE1), a feature that distinguishes eukaryotic MYH from prokaryotic MutY. Of clinical value, our work provides the first structural and biochemical data to implicate impaired cell signaling as another possible mechanism underlying the pathogenic potential of some hMYH mutants in MAP patients.

Materials and Methods

Creation of expression constructs

The sequences of all constructs had been verified before subsequent experiments were undertaken.

hMYH(65–350)

Primers C4F-B and R-EC5 (all of the oligonucleotides used are listed in Table S2) were used to amplify the hMYH (65–350) region of the hMYH gene from the template pET11a-hMYH.[22] The hMYH(65–350) polymerase chain reaction (PCR) product was cleaved by NdeI and XhoI and ligated into a modified pET-19b vector (Novagen) with an N-terminal decahistidine tag and a PreScission Protease cleavage site.

SpMyh1(I261A/E262Q) double mutant

The I261A/E262Q double mutant of the Sp*myh1*$^+$ gene was constructed by PCR splicing overlap extension.[57] Primers CHANG219/Sp-IA-E262Q-R and Sp-IA-E262Q-F/CHANG220 were used to amplify the N-terminal and C-terminal regions of the Sp*myh1*$^+$ gene from the template pET11a-SpMyh1-IA.[39] Next, both purified PCR products were used as templates for another PCR with the CHANG219 and CHANG220 primers. The final PCR products were cleaved by NdeI and BamHI and ligated into the NdeI/BamHI-digested pET11a vector (EMD Biosciences). This parent construct served as the starting point for the subcloning of the SpMyh1-IA/EQ double mutant into a bacterial expression vector for production of the GST-tagged mutant and subcloning into the yeast expression vector pREP41X (American Type Culture Collection). The primers used for the creation of these constructs are listed in Table S2.

GST-SpRad9, GST-SpRad1, and GST-SpHus1

The cDNA fragments containing SpRad9, SpRad1, and SpHus1 fused to the GST gene were obtained by PCR using the primers listed in Table S2 and the templates pET21a-SpRad9, pET21a-SpRad1, and pET21a-SpHus1,[38] respectively. The PCR products were digested with BamHI and ligated into the BamHI-digested vector pGEX-4T-2 GE Healthcare.

SpMyh1 peptide corresponding to residues 245–293 (SpHIP)

The SpHus1 binding region in SpMyh1 has been mapped between residues 245 and 293.[39] For SpHIP expression, the Sp*myh1*$^+$ cDNA fragment coding residues 245–293 was amplified by PCR from full-length cDNA template and pSPMYH19[58] using primers SpMYH245-Xho and SpMYH245-Bam, and ligated into p4X-G, which contains a coding sequence of GFP.[59] Sp*myh1*$^+$ cDNA coding residues 245–293 was also synthesized by PCR with primers SpMYH245-Xho-ATG and SpMYH245-His-Xma and ligated into pREP41X.

MBP-SpMyh1-WT and MBP-SpMyh1-Chimera

Primers TOTH382/SpMyh-F and TOTH371/SpMyh-R were used to amplify the Sp*myh1*$^+$ gene from the template pET11a-SpMyh1. The PCR product was digested with KpnI and BamHI and ligated into a KpnI/BamHI-digested dual N-terminal hexahistidine (His_6)–MBP pLM303 fusion vector.

The SpMyh1-Chimera construct was derived from pET11a-SpMyh1. First, the QuikChange XL Site-Directed Mutagenesis Kit (Stratagene) was used to create a SalI restriction enzyme cut site within the Sp*myh1*$^+$ gene using primers SpMyh-Sal-F and SpMyh-Sal-R. The SalI site was created immediately 3′ to the segment of DNA that encodes for the SpMyh1 IDC region and immediately 5′ to the segment of DNA that encodes for the SpMyh1 C-terminal domain. The pET11a-SpMyh1-SalI mutagenesis product was digested with NdeI and SalI, and the digested DNA fragment containing the pET11a vector and the DNA encoding for the C-terminal domain of SpMyh1 (pET11a-CTDSpMyh1) was gel purified. Simultaneously, PCR was completed to amplify DNA containing a 5′-NdeI cut site and the 5′ end of the Sp*myh1*$^+$ gene up to the beginning of the section of DNA that encodes for the SpMyh1 linker region with primers SpMyh-NdeI and SpMyh-SalI. The SpMyh-SalI primer used in the PCR included DNA to synthesize the specified section of Sp*myh1*$^+$, the EcMutY linker region, and a SalI cut site. This PCR product was digested with NdeI and SalI and ligated into the NdeI-SalI digested pET11a-CTDSpMyh1. With the use of the QuikChange XL Site-Directed Mutagenesis Kit (Stratagene) and primers SpCHIM-Sal-to-Nat-F and SpCHIM-Sal-to-Nat-R, mutagenesis was completed again to remove the SalI site. The pET11a-SpMyh1-Chimera construct was used as template for subcloning into the pLM303 vector.

Protein purification

hMYH(65–350)

hMYH(65–350) was overexpressed in *E. coli* Rosetta™ 2 (DE3) (Novagen) cells. Following cell lysis, the supernatant was loaded onto a nickel-Sepharose (GE Healthcare) affinity column in a buffer containing 50 mM Na_2HPO_4 (pH 8.0), 300 mM NaCl, and 10 mM imidazole. After the column had been washed, hMYH(65–350) was eluted from the column with 250 mM imidazole and then dialyzed at 4 °C overnight in a buffer containing 20 mM KH_2PO_4 (pH 7.4), 300 mM KCl, and 1 mM dithiothreitol (DTT). Subsequently, the protein solution was dialyzed for 2 h in a low-salt buffer (50 mM KCl). hMYH(65–350) was further purified with a Q-Sepharose anion-exchange column (GE Healthcare) using a salt gradient of 0.05–1 M KCl. Most of the protein was retrieved from the flow through and wash. To lower its conductivity, we diluted the hMYH(65–350) collected in a 1:1 ratio with 20 mM KH_2PO_4 (pH 7.4) and 1 mM DTT. Heparin-Sepharose affinity chromatography (GE Healthcare) was used for the final purification step, and the column was developed with a salt gradient of 0.05–1 M KCl. Peak fractions were pooled together and incubated with PreScission Protease (GE Healthcare) in accordance with the manufacturer's instructions, resulting in complete removal of the decahistidine tag. The protein was dialyzed at 4 °C overnight in a buffer containing 50 mM Tris–HCl (pH 7.5), 300 mM NaCl, 1 mM ethylenediaminetetraacetic acid (EDTA), and 1 mM DTT. Purified hMYH(65–350) was concentrated to ~8 mg/ml and stored at −80 °C.

SpMyh1-WT, SpMyh1(I261A), and SpMyh1(I261A/E262Q)

The untagged WT and mutant SpMyh1 proteins were purified in accordance with the described procedures.[58]

MBP-SpMyh1-WT and MBP-SpMyh1-Chimera

The MBP-SpMyh1-WT fusion protein was overexpressed in *E. coli* Rosetta™ 2(DE3) (Novagen) cells. Following cell lysis in the presence of Benzonase (Novagen) nuclease, polyethyleneimine was added to the supernatant to a final concentration of 1% (vol/vol) to precipitate the contaminating nucleic acids. A partial protein purification step was completed with the addition of ammonium sulfate to a final concentration of 30% (wt/vol) to precipitate a subset of the contaminants. Next, ammonium sulfate was added to the remaining solution to a final concentration of 50% (wt/vol) to precipitate MBP-SpMyh1-WT. The precipitated protein was resuspended in buffer T [20 mM Tris–HCl (pH 7.5), 200 mM NaCl, 10 mM β-mercaptoethanol, 0.1 mM EDTA, and 0.1% Triton X-100]. After a 2-h dialysis step in buffer T, the protein was loaded onto an amylose-Sepharose (New England Biolaboratories) affinity column. After the column had been washed, the MBP-fusion protein was eluted from the column with buffer T containing 10 mM maltose. To reduce the ionic strength of the eluted protein sample, we diluted it with buffer H [20 mM KH_2PO_4 (pH 7.5), 1 mM DTT, 0.2 mM phenylmethylsulfonyl fluoride, 10% glycerol, and 0.1% Triton X-100]. A heparin-Sepharose (GE Healthcare) affinity column was used for the final purification step using a salt gradient of 0.05–0.6 M KCl. The peak fractions were pooled, filtered, and stored at −80 °C.

The purification protocol for the MBP-SpMyh1-Chimera fusion protein began in the same way as the protocol used for the MBP-SpMyh1-WT fusion protein. However, after the 2-h dialysis in buffer T, MBP-SpMyh1-Chimera was loaded onto a diethylaminoethyl (DEAE) cellulose (Whatman) anion-exchange column in tandem with the amylose-Sepharose (New England Biolaboratories) affinity column. The DEAE column was used here to bind any remaining contaminating nucleic acids. After a thorough wash step, the DEAE column was removed, and the protein was eluted from the amylose column with buffer T containing 10 mM maltose. To reduce the ionic strength of the eluted protein sample, we diluted it with buffer S [25 nM Hepes (pH 7.5), 1 mM DTT, 0.25 mM EDTA, 1% glycerol, and 0.1% Triton X-100]. At this point, the protein was loaded onto an SP-Sepharose (GE Healthcare) cation-exchange column. The column was developed with a salt gradient of 0.05–1.0 M NaCl. The peak protein fractions were dialyzed for 2 h in buffer Q [20 mM KH_2PO_4 (pH 7.5), 50 mM KCl, 1 mM DTT, and 0.1% Triton X-100]. The final purification step employed anion exchange using a Q-Sepharose (GE Healthcare) anion-exchange column. The Q-Sepharose column was developed with a salt gradient of 0.05–0.6 M KCl. The purified protein was concentrated to about 1.5 mg/ml, filtered, and stored at −80 °C.

Yeast expression

S. pombe *strains and growth*

The yeast strains used in this study are listed in Table S1. Standard procedures and media were used for culture growth, transformation, and genetic analysis.[60] Yeast cells were grown in yeast extract–peptone–dextrose medium for regular maintenance. For specific selection and mutation frequency measurements, cells were grown in Edinburgh minimal medium (EMM) with supplements, as indicated.

Expression of the SpMyh1(I261A/E262Q) mutant in Spmyh1 knockout cells

A clone containing the Sp*myh1* gene (pREP41X-SpI261A/E262Q) was confirmed by DNA sequencing and transformed into Sp*myh1* knockout cells, JSP303-Y4 (*myh1*Δ),[8] by electroporation. Transformed cells acquired a Leu^+ phenotype and were selected on Leu^- yeast nitrogen base (YNB) agar plates. The pREP41X expression vector contains the *nmt1* promoter that can be regulated with varying concentrations of thiamine; transcription at the *nmt1* promoter is almost completely suppressed in the presence of 5 μg/ml thiamine.

Expression of GFP-tagged and His-tagged SpHIP

DNA from a confirmed GFP-SpHIP clone was incorporated via electroporation into the cells of BM2681 or the Hus1-MYC strain, while DNA from a confirmed His-SpHIP clone was incorporated into TMN3309. Transformed GFP-SpHIP cells acquired a Ura^+ phenotype and were selected on Ura^- YNB agar plates. Meanwhile, transformed His-SpHIP cells acquired a Leu^+ phenotype and were selected on Leu^- YNB agar plates.

The transcription of GFP-tagged and His-tagged SpHIP in the expression vectors p4XG and pREP41X, respectively, is controlled by the thiamine-regulated *nmt1* promoter. Yeast cells were grown in EMM to an OD_{600} of ~0.6 in the absence or in the presence of 5 μg/ml thiamine. Cells were harvested and lysed as described previously.[8] The GFP-SpHIP product encoded by the sequences in p4XG was detected by antibodies against either SpMyh1 or GFP. Expression of His-tagged SpHIP in yeast cells was confirmed by Western blot analysis with polyclonal antibodies against full-length SpMyh1, as previously described.[21]

hMYH(65–350) crystallization and structure determination

hMYH(65–350) crystals grew on sitting-drop trays within 1 day in a buffer containing 0.2 M magnesium acetate, 20% (vol/vol) polyethylene glycol 3350, 5 mM Tris[2-carboxyethyl] phosphine, 5% glycerol, and 10 mM spermidine. The crystallization buffer was supplemented with glycerol to a final concentration of 20% (vol/vol) for cryoprotection. The crystals are primitive monoclinic ($P2_1$), with cell dimensions $a = 60.31$ Å, $b = 82.17$ Å, $c = 63.46$ Å, and $\beta = 100.9$, and contain a dimer in the asymmetric unit. X-ray diffraction data were collected at beamline X6A in the National Synchrotron Light Source of the Brookhaven National Laboratory. The images were processed and scaled using the HKL2000 program suite.[61] The [4Fe–4S] cluster within hMYHΔC5 enabled the collection of single-wavelength anomalous diffraction data at the iron absorption edge [1.65 Å (7.5 keV)] to 2.3 Å resolution. Computational programs within the Collaborative Computational Program Number 4[62] were used for structure determination. The positions of the two [4Fe–4S] clusters in the asymmetric unit were determined

by inspection of an anomalous difference Patterson map. After phasing and density modification, the resulting electron density maps were not of sufficient quality to allow model building to proceed. Thus, a combined approach using both experimental phases derived from iron positions and molecular replacement was employed. The Collaborative Computational Program Number 4 program CHAINSAW was used to generate a search model from the EcMutY structure. Two rounds of molecular replacement were needed to obtain a solution for both hMYH(65–350) monomers in the asymmetric unit. Using the experimental phases of hMYH(65–350) from MLPHARE and the EcMutY search model, we found one monomer of hMYH(65–350) with MOLREP, which determined the position of the second monomer. The model phases from this molecular replacement solution were used to complete rigid-body refinement in REFMAC. The resulting model phases were used to initiate a second round of molecular replacement in MOLREP. Model building was carried out with the program Coot. Additional noncrystallographic symmetry averaging was performed using noncrystallographic symmetry operators derived from the correctly placed search model, along with solvent flattening and histogram matching with the program DM. The density-modified phases were used as input for restraints for the REFMAC mlhl target function. Additionally, TLS refinement was performed on the catalytic domain and the IDC as separate domains. After several rounds of model building and addition of waters, the R_{free} was 25.1%, and the R_{cryst} was 20.6%. The data collection and refinement statistics are presented in Table 1. Analysis of the Ramachandran plot shows that 94.4% of residues are in favored regions and 5.6% of residues are in allowed regions. Figures were made using the program PyMOL.[63]

Glycosylase activity assays of SpMyh1 proteins

The glycosylase assay for purified recombinant SpMyh1 and for the SpMyh1(I261A/E262Q) double mutant with an A/8-oxoG-containing DNA substrate was described previously.[58] The DNA substrate was a 20-bp duplex DNA containing a central A/8-oxoG mismatch. The *S. pombe* 9-1-1 complex was purified as described previously.[39] The glycosylase assay for purified SpMyh1-Chimera followed the same protocol, except that the glycosylase reaction was performed at 25 °C instead of 30 °C.

Glycosylase assay of hMYH(65–350)

The glycosylase assay for purified recombinant hMYH (65–350) was similar to the assay described previously,[24] except that a different DNA substrate and different incubation times were used. The DNA substrate was a 20-bp duplex DNA containing a central A/8-oxoG mismatch. The DNA strand containing the adenine was 5′ labeled with fluorescein ^{32}P. The hMYH glycosylase reaction mixtures were incubated for 30 min at 37 °C. The reactions were stopped by heating the samples with NaOH to a final concentration of 0.1 M for 30 min at 90 °C.

GST pull-down assay

Expression and immobilization of GST fusion constructs and the GST pull-down assay were similar to the procedures described previously.[38] *E. coli* (BL21Star/DE3) cells (Stratagene) harboring the expression plasmids were cultured in Luria–Bertani broth containing 100 μg/ml ampicillin at 25 °C. Protein expression was induced as described above. Cell paste from a 0.5-l culture was lysed, and extracts were immobilized onto glutathione-Sepharose 4B (GE Healthcare). A control was run concurrently with immobilized GST alone. After the pellets had been washed, they were fractionated on a 10% (for His-tagged SpHus1) or 20% (for SpHIP) SDS polyacrylamide gel and transferred to a nitrocellulose membrane. Western blot analyses were performed with antibody against His tag (sc-8036; Santa Cruz Biotechnology) or SpMyh1.[8]

Coimmunoprecipitation of GFP-SpHIP with SpHus1 protein

GFP-SpHIP expressed in Hus1-MYC cells was precipitated by an anti-GFP antibody. Extracts (1 mg) derived from *S. pombe* cells expressing GFP alone or GFP-SpHIP were precleared by incubation with protein A Sepharose (50 μl) in phosphate-buffered saline with protease inhibitors (Sigma-Aldrich) for 4 h at 4 °C. After removal of the beads, the supernatant was mixed with 4 μl of monoclonal anti-GFP antibody (Abcam) for 16 h at 4 °C. Then, protein A Sepharose (50 μl) was added to precipitate GFP-SpHIP. After centrifugation at 1000*g*, the supernatant was collected, and the pellets were washed. Both the supernatant (10% of the total volume) and pellet fractions were resolved on a 12% SDS-PAGE gel. The Myc-tagged SpHus1 that coprecipitated with GFP-SpHIP was verified with Western blot analysis using antibodies against c-Myc (Santa Cruz Biotechnology).

Measurement of mutation frequency

A clone containing the Sp*myh1* gene (pREP41X-SpI261A/E262Q) was transformed into Sp*myh1* knockout cells, JSP303-Y4 (*myh1*Δ),[8] by electroporation. Five independent yeast colonies were grown to late log phase in EMM containing 0.1 mg/ml uracil. Additional amino acids were supplemented for the WT strain (0.1 mg/ml Leu and His) and the *myh1*Δ strain (0.1 mg/ml Leu). Each culture was plated onto EMM agar plates containing 1 mg/ml 5-fluoro-orotic acid (FOA) and 0.1 mg/ml uracil. FOA-resistant colonies were counted after 5 days of growth. The cell titer was determined by plating 0.1 ml of a 10^{-4} dilution onto plates without FOA. The mutation frequency was calculated as the ratio of FOA-resistant cells to the total cells. The measurement was repeated at least three times to ensure reproducibility.

H_2O_2 treatment

For H_2O_2 treatment, 1.0 ml of an overnight yeast culture grown in EMM containing 5 μg/ml thiamine was added to 20 ml of EMM in the absence or in the presence of 5 μg/ml thiamine. At an OD_{600} of ~0.6, 2 ml of the culture was aliquoted into 30-ml test tubes, followed by addition of H_2O_2 to each aliquot at various concentrations. After a 30-min incubation step, the cells were pelleted and resuspended in fresh H_2O_2-free medium and shaken at 32 °C for 1 h or 2 h. Cells were diluted 10,000-fold and plated on yeast extract–peptone–dextrose plates. The

number of colonies was scored after 3 days of incubation at 32 °C.

Measurement of DNA binding affinity via fluorescence anisotropy

Fluorescence anisotropy experiments were performed to measure the affinity of SpMhy1 or SpMyh1-Chimera for a 20-bp duplex DNA substrate containing a centrally located abasic site opposite an 8-oxoG nucleotide on the complementary strand. The DNA substrate was prepared by 5′ labeling the strand containing the abasic site with fluorescein (Integrated DNA Technologies). The binding experiments were conducted as described previously[64] using 1 nM labeled DNA. For SpMyh1, total fluorescence emission decreased as a function of added protein concentration requiring that an appropriate correction factor[64] be applied to the measured anisotropies. Relative affinities were calculated from binding isotherms using the program GraphPad Prism version 3.03 and a variant of the Hill equation:[64,65]

$$A_{\text{total}} = A_{\text{DNA}} + \left[\left(A_{\text{comp}} - A_{\text{DNA}}\right) \left(\frac{\left([\text{P}]/[\text{P}]_{\text{m}}\right)^{h}}{1 + \left([\text{P}]/[\text{P}]_{\text{m}}\right)^{h}} \right) \right] \quad (1)$$

where A_{total} is the measured anisotropy, A_{DNA} is the inherent anisotropy of the DNA substrate, A_{comp} is the anisotropy of the saturated protein–DNA complex, and h is the Hill coefficient. This equation also estimates the midpoint of the binding isotherm ($[\text{P}]_{\text{m}}$), which, in the case of a single binding site (i.e., h is constrained to be 1.0), is equivalent to K_{d}. To determine the affinity for undamaged DNA, we used the identical method, with the exception that the substrate was a 19-bp duplex DNA substrate with a centrally located C:G base pair, with one base overhanging at the 5′ end of the DNA strand containing guanine.

Competition assay

To determine the substrate specificity of SpMyh1-Chimera, we measured the ability of competitor DNA substrates to displace an A/8-oxoG substrate bound to the glycosylase. We used a fluorescein-labeled 20-bp duplex DNA with a centrally located A/8-oxoG mispair. The strand containing the adenine was 5′ labeled with fluorescein (Integrated DNA Technologies). The experiments also required the use of unlabeled 20-bp duplex DNA substrates with either a centrally located C:G pair or an A/8-oxoG mispair. Reaction samples included 150 nM of either SpMyh1-Chimera or MBP-SpMyh1-WT, 1 nM 5′-fluorescein-labeled 20-bp duplex DNA, and either the C:G or the A/8-oxoG unlabeled 20-bp duplex DNA substrate over a range of concentrations (0–1000 nM) (Fig. 6d). The reaction samples were preincubated in low-ionic-strength buffer for 30 min at 25 °C to allow the samples to reach equilibrium before the measurement of A/8-oxoG binding to SpMyh1-Chimera or MBP-SpMyh1-WT in the presence of the unlabeled duplex DNA competitor with either the C:G pair or the A/8-oxoG mispair. The measured anisotropy values were analyzed as a function of competitor DNA concentration, similar to what was described previously.[64] Plots of anisotropy *versus* competitor concentration were made to measure apparent inhibition constants ($K_{\text{i,app}}$) for the competitor DNA substrates. $K_{\text{i,app}}$ measurements were calculated using the equation:[64]

$$A_{\text{total}} = A_{\text{DNA}} + \frac{A_{\text{max}}}{1 + \left([\text{I}] / K_{\text{i,app}}\right)} \quad (2)$$

where A_{total} is the measured anisotropy, A_{DNA} is the anisotropy of the labeled DNA alone, A_{max} is the maximum observed anisotropy shift (i.e., in the absence of competitor DNA), and [I] is the concentration of the competitor DNA. The $K_{\text{i,app}}$ measurements estimate the competitor DNA concentrations needed to achieve half maximal binding to SpMyh1-Chimera or MBP-SpMyh1-WT.

Accession numbers

The coordinates for the structure of hMYH(65–350) have been deposited in the Protein Data Bank with accession code 3N5N.

Acknowledgements

We thank Dr. Antony Carr (MRC Cell Mutation Unit, UK), Dr. Charles Hoffman (Boston College), and Dr. Paul Russell (The Scripps Research Institute) for kindly providing the *S. pombe* strains. We are grateful to Dr. Emma Warbrick (University of Dundee, UK) for providing the plasmid p4XG. We acknowledge Dr. Laura Mizoue (Center for Structural Biology at Vanderbilt University) for providing the expression plasmid used to produce recombinant SpMyh1-WT and SpMyh1-Chimera proteins. We also thank the staff of the University of Maryland Marlene and Stewart Greenebaum Cancer Center Structural Biology Shared Service and the staff of beamline X6A at National Synchrotron Light Source of the Brookhaven National Laboratory for assistance with X-ray data collection. Our initial efforts were supported by institutional research grant IRG-97-153-07 from the American Cancer Society (to Alan Tomkinson). This work was further supported by grants GM35132 and CA78391 from the National Institutes of Health (to A.L.) and by grant RSG-09-058-01-GMC from the American Cancer Society (to E.A.T.).

Supplementary Data

Supplementary data associated with this article can be found, in the online version, at doi:10.1016/j.jmb.2010.08.045

References

1. Lindahl, T. & Wood, R. D. (1999). Quality control by DNA repair. *Science*, **286**, 1897–1905.

2. Collins, A. R. (1999). Oxidative DNA damage, antioxidants, and cancer. *BioEssays*, **21**, 238–246.
3. Shibutani, S., Takeshita, M. & Grollman, A. P. (1991). Insertion of specific bases during DNA synthesis past the oxidation-damaged base 8-oxodG. *Nature*, **349**, 431–434.
4. Moriya, M. & Grollman, A. P. (1993). Mutations in the mutY gene of *Escherichia coli* enhance the frequency of targeted G:C→T:A transversions induced by a single 8-oxoguanine residue in single-stranded DNA. *Mol. Gen. Genet.* **239**, 72–76.
5. Wood, M. L., Dizdaroglu, M., Gajewski, E. & Essigmann, J. M. (1990). Mechanistic studies of ionizing radiation and oxidative mutagenesis: genetic effects of a single 8-hydroxyguanine (7-hydro-8-oxoguanine) residue inserted at a unique site in a viral genome. *Biochemistry*, **29**, 7024–7032.
6. Lu, A. L., Li, X., Gu, Y., Wright, P. M. & Chang, D. Y. (2001). Repair of oxidative DNA damage: mechanisms and functions. *Cell Biochem. Biophys.* **35**, 141–170.
7. Mol, C. D., Parikh, S. S., Putnam, C. D., Lo, T. P. & Tainer, J. A. (1999). DNA repair mechanisms for the recognition and removal of damaged DNA bases. *Annu. Rev. Biophys. Biomol. Struct.* **28**, 101–128.
8. Chang, D. Y., Gu, Y. & Lu, A. L. (2001). Fission yeast (*Schizosaccharomyces pombe*) cells defective in the MutY-homologous glycosylase activity have a mutator phenotype and are sensitive to hydrogen peroxide. *Mol. Genet. Genomics*, **266**, 336–342.
9. Hirano, S., Tominaga, Y., Ichinoe, A., Ushijima, Y., Tsuchimoto, D., Honda-Ohnishi, Y. *et al.* (2003). Mutator phenotype of MUTYH-null mouse embryonic stem cells. *J. Biol. Chem.* **278**, 38121–38124.
10. Al-Tassan, N., Chmiel, N. H., Maynard, J., Fleming, N., Livingston, A. L., Williams, G. T. *et al.* (2002). Inherited variants of MYH associated with somatic G:C→T:A mutations in colorectal tumors. *Nat. Genet.* **30**, 227–232.
11. Halford, S. E., Rowan, A. J., Lipton, L., Sieber, O. M., Pack, K., Thomas, H. J. *et al.* (2003). Germline mutations but not somatic changes at the MYH locus contribute to the pathogenesis of unselected colorectal cancers. *Am. J. Pathol.* **162**, 1545–1548.
12. Jones, S., Emmerson, P., Maynard, J., Best, J. M., Jordan, S. & Williams, G. T. (2002). Biallelic germline mutations in MYH predispose to multiple colorectal adenoma and somatic G:C→T:A mutations. *Hum. Mol. Genet.* **11**, 2961–2967.
13. Sampson, J. R., Dolwani, S., Jones, S., Eccles, D., Ellis, A., Evans, D. G. *et al.* (2003). Autosomal recessive colorectal adenomatous polyposis due to inherited mutations of MYH. *Lancet*, **362**, 39–41.
14. Cheadle, J. P. & Sampson, J. R. (2007). MUTYH-associated polyposis—from defect in base excision repair to clinical genetic testing. *DNA Repair (Amsterdam)*, **6**, 274–279.
15. Kundu, S., Brinkmeyer, M. K., Livingston, A. L. & David, S. S. (2009). Adenine removal activity and bacterial complementation with the human MutY homologue (MUTYH) and Y165C, G382D, P391L and Q324R variants associated with colorectal cancer. *DNA Repair (Amsterdam)*, **8**, 1400–1410.
16. Bai, H., Grist, S., Gardner, J., Suthers, G., Wilson, T. M. & Lu, A. L. (2007). Functional characterization of human MutY homolog (hMYH) missense mutation (R231L) that is linked with hMYH-associated polyposis. *Cancer Lett.* **250**, 74–81.
17. Molatore, S., Russo, M. T., D'Agostino, V. G., Barone, F., Matsumoto, Y., Albertini, A. M. *et al.* (2010). MUTYH mutations associated with familial adenomatous polyposis: functional characterization by a mammalian cell-based assay. *Hum. Mutat.* **31**, 159–166.
18. Bai, H., Jones, S., Guan, X., Wilson, T. M., Sampson, J. R., Cheadle, J. P. & Lu, A. L. (2005). Functional characterization of two human MutY homolog (hMYH) missense mutations (R227W and V232F) that lie within the putative hMSH6 binding domain and are associated with hMYH polyposis. *Nucleic Acids Res.* **33**, 597–604.
19. Bellacosa, A. (2001). Functional interactions and signaling properties of mammalian DNA mismatch repair proteins. *Cell Death Differ.* **8**, 1076–1092.
20. Sancar, A., Lindsey-Boltz, L. A., Unsal-Kacmaz, K. & Linn, S. (2004). Molecular mechanisms of mammalian DNA repair and the DNA damage checkpoints. *Annu. Rev. Biochem.* **73**, 39–85.
21. Chang, D. Y. & Lu, A. L. (2002). Functional interaction of MutY homolog with proliferating cell nuclear antigen in fission yeast, *Schizosaccharomyces pombe*. *J. Biol. Chem.* **277**, 11853–11858.
22. Parker, A., Gu, Y., Mahoney, W., Lee, S. H., Singh, K. K. & Lu, A. L. (2001). Human homolog of the MutY repair protein (hMYH) physically interacts with proteins involved in long patch DNA base excision repair. *J. Biol. Chem.* **276**, 5547–5555.
23. Boldogh, I., Milligan, D., Lee, M. S., Bassett, H., Lloyd, R. S. & McCullough, A. K. (2001). hMYH cell cycle-dependent expression, subcellular localization and association with replication foci: evidence suggesting replication-coupled repair of adenine:8-oxoguanine mispairs. *Nucleic Acids Res.* **29**, 2802–2809.
24. Gu, Y., Parker, A., Wilson, T. M., Bai, H., Chang, D. Y. & Lu, A. L. (2002). Human MutY homolog, a DNA glycosylase involved in base excision repair, physically and functionally interacts with mismatch repair proteins human MutS homolog 2/human MutS homolog 6. *J. Biol. Chem.* **277**, 11135–11142.
25. Hayashi, H., Tominaga, Y., Hirano, S., McKenna, A. E., Nakabeppu, Y. & Matsumoto, Y. (2002). Replication-associated repair of adenine:8-oxoguanine mispairs by MYH. *Curr. Biol.* **12**, 335–339.
26. Murakami, H. & Nurse, P. (2000). DNA replication and damage checkpoints and meiotic cell cycle controls in the fission and budding yeasts. *Biochem. J.* **349**, 1–12.
27. Weinert, T. (1998). DNA damage checkpoints update: getting molecular. *Curr. Opin. Genet. Dev.* **8**, 185–193.
28. Dore, A. S., Kilkenny, M. L., Rzechorzek, N. J. & Pearl, L. H. (2009). Crystal structure of the Rad9–Rad1–Hus1 DNA damage checkpoint complex—implications for clamp loading and regulation. *Mol. Cell*, **34**, 735–745.
29. Sohn, S. Y. & Cho, Y. (2009). Crystal structure of the human rad9–hus1–rad1 clamp. *J. Mol. Biol.* **390**, 490–502.
30. Xu, M., Bai, L., Gong, Y., Xie, W., Hang, H. & Jiang, T. (2009). Structure and functional implications of the

human rad9–hus1–rad1 cell cycle checkpoint complex. *J. Biol. Chem.* **284**, 20457–20461.
31. Burtelow, M. A., Roos-Mattjus, P. M., Rauen, M., Babendure, J. R. & Karnitz, L. M. (2001). Reconstitution and molecular analysis of the hRad9–hHus1–hRad1 (9-1-1) DNA damage responsive checkpoint complex. *J. Biol. Chem.* **276**, 25903–25909.
32. Shiomi, Y., Shinozaki, A., Nakada, D., Sugimoto, K., Usukura, J., Obuse, C. & Tsurimoto, T. (2002). Clamp and clamp loader structures of the human checkpoint protein complexes, Rad9-1-1 and Rad17-RFC. *Genes Cells*, **7**, 861–868.
33. Venclovas, C. & Thelen, M. P. (2000). Structure-based predictions of Rad1, Rad9, Hus1 and Rad17 participation in sliding clamp and clamp-loading complexes. *Nucleic Acids Res.* **28**, 2481–2493.
34. al-Khodairy, F. & Carr, A. M. (1992). DNA repair mutants defining G2 checkpoint pathways in *Schizosaccharomyces pombe*. *EMBO J.* **11**, 1343–1350.
35. al-Khodairy, F., Fotou, E., Sheldrick, K. S., Griffiths, D. J., Lehmann, A. R. & Carr, A. M. (1994). Identification and characterization of new elements involved in checkpoint and feedback controls in fission yeast. *Mol. Biol. Cell*, **5**, 147–160.
36. Zou, L., Cortez, D. & Elledge, S. J. (2002). Regulation of ATR substrate selection by Rad17-dependent loading of Rad9 complexes onto chromatin. *Genes Dev.* **16**, 198–208.
37. Lu, A. L., Bai, H., Shi, G. & Chang, D. Y. (2006). MutY and MutY homologs (MYH) in genome maintenance. *Front. Biosci.* **11**, 3062–3080.
38. Chang, D. Y. & Lu, A. L. (2005). Interaction of checkpoint proteins Hus1/Rad1/Rad9 with DNA base excision repair enzyme MutY homolog in fission yeast, *Schizosaccharomyces pombe*. *J. Biol. Chem.* **280**, 408–417.
39. Shi, G., Chang, D. Y., Cheng, C. C., Guan, X., Venclovas, C. & Lu, A. L. (2006). Physical and functional interactions between MutY glycosylase homologue (MYH) and checkpoint proteins Rad9–Rad1–Hus1. *Biochem. J.* **400**, 53–62.
40. Hartwell, L. H. & Kastan, M. B. (1994). Cell cycle control and cancer. *Science*, **266**, 1821–1828.
41. Fromme, J. C., Banerjee, A., Huang, S. J. & Verdine, G. L. (2004). Structural basis for removal of adenine mispaired with 8-oxoguanine by MutY adenine DNA glycosylase. *Nature*, **427**, 652–656.
42. Guan, Y., Manuel, R. C., Arvai, A. S., Parikh, S. S., Mol, C. D., Miller, J. H. *et al.* (1998). MutY catalytic core, mutant and bound adenine structures define specificity for DNA repair enzyme superfamily. *Nat. Struct. Biol.* **5**, 1058–1064.
43. Noll, D. M., Gogos, A., Granek, J. A. & Clarke, N. D. (1999). The C-terminal domain of the adenine-DNA glycosylase MutY confers specificity for 8-oxoguanine·adenine mispairs and may have evolved from MutT, an 8-oxo-dGTPase. *Biochemistry*, **38**, 6374–6379.
44. Volk, D. E., House, P. G., Thiviyanathan, V., Luxon, B. A., Zhang, S., Lloyd, R. S. & Gorenstein, D. G. (2000). Structural similarities between MutT and the C-terminal domain of MutY. *Biochemistry*, **39**, 7331–7336.
45. Gogos, A., Cillo, J., Clarke, N. D. & Lu, A. L. (1996). Specific recognition of A/G and A/7,8-dihydro-8-oxoguanine (8-oxoG) mismatches by *Escherichia coli* MutY: removal of the C-terminal domain preferentially affects A/8-oxoG recognition. *Biochemistry*, **35**, 16665–16671.
46. Li, X., Wright, P. M. & Lu, A. L. (2000). The C-terminal domain of MutY glycosylase determines the 7,8-dihydro-8-oxo-guanine specificity and is crucial for mutation avoidance. *J. Biol. Chem.* **275**, 8448–8455.
47. Lee, S. & Verdine, G. L. (2009). Atomic substitution reveals the structural basis for substrate adenine recognition and removal by adenine DNA glycosylase. *Proc. Natl Acad. Sci. USA*, **106**, 18497–18502.
48. Chmiel, N. H., Golinelli, M. P., Francis, A. W. & David, S. S. (2001). Efficient recognition of substrates and substrate analogs by the adenine glycosylase MutY requires the C-terminal domain. *Nucleic Acids Res.* **29**, 553–564.
49. Manuel, R. C. & Lloyd, R. S. (1997). Cloning, overexpression, and biochemical characterization of the catalytic domain of MutY. *Biochemistry*, **36**, 11140–11152.
50. Arnold, K., Bordoli, L., Kopp, J. & Schwede, T. (2006). The SWISS-MODEL workspace: a Web-based environment for protein structure homology modelling. *Bioinformatics*, **22**, 195–201.
51. Yang, H., Clendenin, W. M., Wong, D., Demple, B., Slupska, M. M., Chiang, J. H. & Miller, J. H. (2001). Enhanced activity of adenine-DNA glycosylase (Myh) by apurinic/apyrimidinic endonuclease (Ape1) in mammalian base excision repair of an A/GO mismatch. *Nucleic Acids Res.* **29**, 743–752.
52. Helt, C. E., Wang, W., Keng, P. C. & Bambara, R. A. (2005). Evidence that DNA damage detection machinery participates in DNA repair. *Cell Cycle*, **4**, 529–532.
53. Doublie, S., Bandaru, V., Bond, J. P. & Wallace, S. S. (2004). The crystal structure of human endonuclease VIII-like 1 (NEIL1) reveals a zincless finger motif required for glycosylase activity. *Proc. Natl Acad. Sci. USA*, **101**, 10284–10289.
54. Smet-Nocca, C., Wieruszeski, J. M., Chaar, V., Leroy, A. & Benecke, A. (2008). The thymine-DNA glycosylase regulatory domain: residual structure and DNA binding. *Biochemistry*, **47**, 6519–6530.
55. Dyson, H. J. & Wright, P. E. (2005). Intrinsically unstructured proteins and their functions. *Nat. Rev. Mol. Cell Biol.* **6**, 197–208.
56. Manuel, R. C., Czerwinski, E. W. & Lloyd, R. S. (1996). Identification of the structural and functional domains of MutY, an *Escherichia coli* DNA mismatch repair enzyme. *J. Biol. Chem.* **271**, 16218–16226.
57. Ho, S. N., Hunt, H. D., Horton, R. M., Pullen, J. K. & Pease, L. R. (1989). Site-directed mutagenesis by overlap extension using the polymerase chain reaction. *Gene*, **77**, 51–59.
58. Lu, A. L. & Fawcett, W. P. (1998). Characterization of the recombinant MutY homolog, an adenine DNA glycosylase, from yeast *Schizosaccharomyces pombe*. *J. Biol. Chem.* **273**, 25098–25105.
59. Warbrick, E. (2006). A functional analysis of PCNA-binding peptides derived from protein sequence, interaction screening and rational design. *Oncogene*, **25**, 2850–2859.

60. Moreno, S., Klar, A. & Nurse, P. (1991). Molecular genetic analysis of fission yeast *Schizosaccharomyces pombe*. *Methods Enzymol.* **194**, 795–823.
61. Otwinowski, Z. & Minor, W. (1997). Processing of X-ray diffraction data collected in oscillation mode. *Methods Enzymol.* **276**, 307–326.
62. The CCP4 suite: programs for protein crystallography. *Acta Crystallogr. Sect. D*, **50**. (1994)., 760–763.
63. DeLano, W. L. (2008). *The PyMOL Molecular Graphics System.* DeLano Scientific LLC, Palo Alto, CA.
64. Bernstein, J., Patterson, D. N., Wilson, G. M. & Toth, E. A. (2008). Characterization of the essential activities of *Saccharomyces cerevisiae* Mtr4p, a 3′→5′ helicase partner of the nuclear exosome. *J. Biol. Chem.* **283**, 4930–4942.
65. Heilman-Miller, S. L., Thirumalai, D. & Woodson, S. A. (2001). Role of counterion condensation in folding of the *Tetrahymena* ribozyme: I. Equilibrium stabilization by cations. *J. Mol. Biol.* **306**, 1157–1166.